



OPEN

NLRP3 licenses NLRP11 for inflammasome activation in human macrophages

Anu Gangopadhyay^{1,2,5,8}, Savita Devi^{1,8}, Shivendra Tenguria^{1,8}, Jessica Carriere¹, Huyen Nguyen¹, Elisabeth Jäger¹, Hemisha Khatri¹, Lan H. Chu^{2,6}, Rojo A. Ratsimandresy^{1,7}, Andrea Dorfleutner^{1,3}✉ and Christian Stehlik^{1,3,4}✉

Intracellular sensing of stress and danger signals initiates inflammatory innate immune responses by triggering inflammasome assembly, caspase-1 activation and pyroptotic cell death as well as the release of interleukin 1 β (IL-1 β), IL-18 and danger signals. NLRP3 broadly senses infectious patterns and sterile danger signals, resulting in the tightly coordinated and regulated assembly of the NLRP3 inflammasome, but the precise mechanisms are incompletely understood. Here, we identified NLRP11 as an essential component of the NLRP3 inflammasome in human macrophages. NLRP11 interacted with NLRP3 and ASC, and deletion of NLRP11 specifically prevented NLRP3 inflammasome activation by preventing inflammasome assembly, NLRP3 and ASC polymerization, caspase-1 activation, pyroptosis and cytokine release but did not affect other inflammasomes. Restored expression of NLRP11, but not NLRP11 lacking the PYRIN domain (PYD), restored inflammasome activation. NLRP11 was also necessary for inflammasome responses driven by NLRP3 mutations that cause cryopyrin-associated periodic syndrome (CAPS). Because NLRP11 is not expressed in mice, our observations emphasize the specific complexity of inflammasome regulation in humans.

Germline-encoded, cytosolic pattern recognition receptors sense infectious and sterile stress signals and play a key role in mounting an inflammatory response that eradicates infections and facilitates wound healing and homeostasis. A consequence of intracellular pattern recognition is the activation of caspase-1 within the inflammasome^{1,2}, and NOD-like receptor (NLR) family pyrin domain containing 3 (NLRP3) is a prominent inflammasome sensor of microbial patterns, self-derived danger signals and environmental cues^{3–5}. Excessive or mutation-driven NLRP3 responses cause a wide range of inflammatory diseases⁶, including CAPS, which is caused by gain-of-function mutations in *NLRP3* (ref. 7). NLRP3 consists of an N-terminal PYD, a central NAIP [neuronal apoptosis inhibitor protein], C2TA [class 2 transcription activator, of the MHC], HET-E [heterokaryon incompatibility] and TP1 [telomerase-associated protein 1] (NACHT) domain and C-terminal leucine-rich regions (LRRs). The NACHT has ATPase activity and is bound to the LRRs and/or the PYD to maintain an inactive conformation^{8,9}. Once this autoinhibition is released, NLRP3 oligomerizes, and its PYD nucleates polymerization of the adaptor protein ASC, which serves as an amplification mechanism and proceeds in a prion-like, self-perpetuating manner, establishing a temporal-spatial threshold control^{10–12}. Polymerized ASC filaments eventually assemble into the characteristic single macromolecular aggregate (speck)^{13,14}. ASC polymerization in turn nucleates caspase-1 polymerization by caspase recruitment domain (CARD)–CARD interactions, resulting in its induced, proximity-mediated activation¹⁵. Caspase-1 is ultimately responsible for the induction of pyroptosis through the cleavage of gasdermin D (GSDMD) and

subsequent GSDMD pore formation, maturation and release of the proinflammatory cytokines IL-1 β and IL-18 and the release of danger signals, including IL-1 α , HMGB1 and polymerized ASC particles^{16–18}. NLRP3 inflammasome activation proceeds in two steps. Priming includes the upregulation of inflammasome components, including NLRP3 and the substrate IL-1 β , a metabolic shift from oxidative phosphorylation to glycolysis and the post-translational modifications of NLRP3, ASC and caspase-1 (refs. 3–5). NLRP3 is activated by diverse stimuli³, and K⁺ efflux has been proposed as the unifying mechanism for NLRP3 activation¹⁹. Protein oligomerization is a common mechanism for the activation of innate immune signaling and NLRP3 oligomerization, and particularly the downstream ASC polymerization, are key events in inflammasome activation^{10,11}. Among the NLRP3 regulatory proteins, NEK7 promotes inflammasome activation by bridging two NLRP3 molecules, which is insufficient to induce NLRP3 oligomerization^{20–23}. GBP5 enables NLRP3–ASC binding in response to soluble, but not crystalline, agonists²⁴, implying that other crucial, yet-unknown cofactors are necessary for NLRP3 oligomerization, inflammasome assembly and activation. To date, the precise mechanism, especially in humans, remains unclear.

Here, we report the identification of NLRP11 as an NLRP3 inflammasome component in human macrophages. NLRP11 bound to ASC and NLRP3 and was required for NLRP3 oligomerization and ASC polymerization. In the absence of NLRP11, NLRP3-mediated caspase-1 activation and release of IL-1 β and IL-18 were defective, but activation of AIM2, NLRC4 and NLRP7 inflammasomes was not affected. The NLRP3–ASC–NLRP11

¹Department of Academic Pathology, Cedars Sinai Medical Center, Los Angeles, CA, USA. ²Driskill Graduate Program in Life Sciences, Feinberg School of Medicine, Northwestern University, Chicago, IL, USA. ³Department of Biomedical Sciences, Cedars Sinai Medical Center, Los Angeles, CA, USA. ⁴Samuel Oschin Comprehensive Cancer Institute, Cedars Sinai Medical Center, Los Angeles, CA, USA. ⁵Present address: SyntheKine, Menlo Park, CA, USA. ⁶Present address: Department of Immunology, University of Washington, Seattle, WA, USA. ⁷Present address: Department of Immunology, Genentech, South San Francisco, CA, USA. ⁸These authors contributed equally: Anu Gangopadhyay, Savita Devi, Shivendra Tenguria. ✉e-mail: andrea.dorfleutner@cshs.org; christian.stehlik@csmc.edu

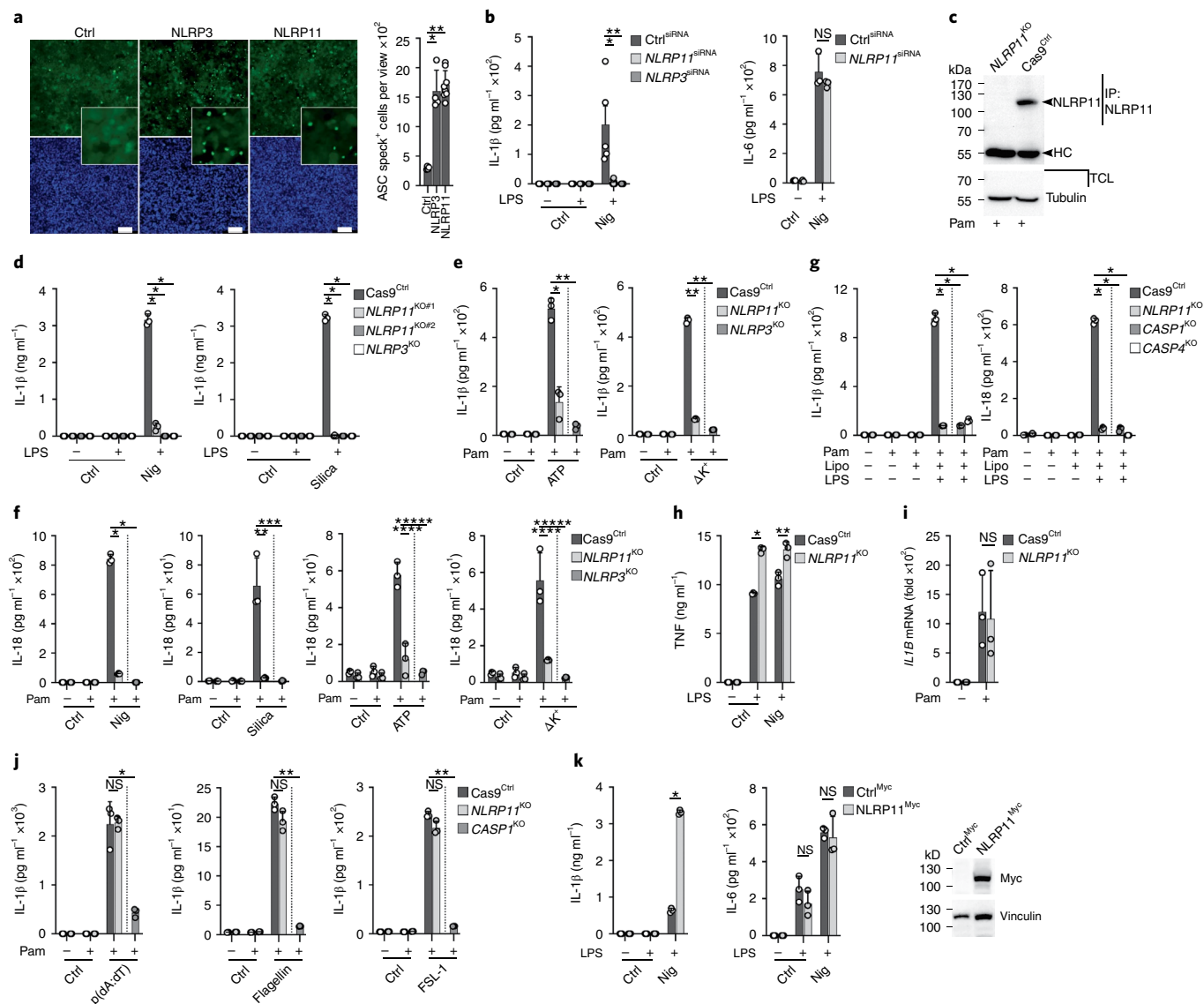


Fig. 1 | NLRP11 is required for NLRP3-mediated cytokine release. **a**, Fluorescence microscopy of EGFP (green) and 4,6-diamidino-2-phenylindole (DAPI) (blue) in HEK293^{ASC-EGFP} cells transiently transfected with empty plasmid (Ctrl), NLRP3 or NLRP11 (left) and quantification of ASC speck⁺ cells/view (right) (Ctrl: $n=4$, NLRP3: $n=4$, NLRP11: $n=8$; mean \pm standard deviation (s.d.)); $*P=0.0003$, $**P<0.0001$. scale bars, 100 μm . **b**, IL-1 β and IL-6 enzyme-linked immunosorbent assay (ELISA) of cleared culture supernatant (SN) from human macrophages transfected with Ctrl^{siRNA}, NLRP11^{siRNA} or NLRP3^{siRNA}: left untreated; primed with LPS (200 ng ml⁻¹, 4 h) and primed and activated with nigericin (Nig) (5 μM , 30 min) (IL-1 β : $n=5$, IL-6: $n=3$, mean \pm s.d.); $*P=0.0043$, $**P=0.0079$. **c**, Immunoprecipitation (IP) with immobilized anti-NLRP11 antibodies using total cell lysates (TCLs) from Cas9^{Ctrl} and NLRP11^{KO} THP-1 cells primed with Pam3CSK4 (Pam) (1 $\mu\text{g ml}^{-1}$, 4 h) and analysis by immunoblot alongside TCL for NLRP11 and tubulin loading control. The arrowheads mark NLRP11 and immunoglobulin G heavy chain (HC). **d-f**, IL-1 β (d,e) and IL-18 (f) ELISA of SN from Cas9^{Ctrl}, NLRP11^{KO#1}, NLRP11^{KO#2} and NLRP3^{KO} cells left untreated, primed with LPS (200 ng ml⁻¹, 4 h) or Pam3CSK4 (1 $\mu\text{g ml}^{-1}$, 4 h) and primed and activated with nigericin (5 μM , 30 min), silica (200 $\mu\text{g ml}^{-1}$, 6 h), ATP (5 mM, 25 min) or cultured in K⁺-free medium (3 h) ($n=3$, mean \pm s.d.). $*P<0.0001$ (d), $*P=0.0009$, $**P<0.0001$ (e); $*P<0.0001$, $**P=0.0044$, $***P=0.0039$, $****P=0.002$, $*****P=0.0002$, $*****P=0.0077$, $*****P=0.0037$ (f). The dotted line indicates that for NLRP3^{KO} only the Pam3CSK4 + nigericin group is shown as control. **g**, IL-1 β and IL-18 ELISA of SN from Cas9^{Ctrl}, NLRP11^{KO}, CASP4^{KO} or CASP4^{KO} cells left untreated, primed with Pam3CSK4 (1 $\mu\text{g ml}^{-1}$, 4 h) and Lipofectamine 2000 (Lipo) transfected with or without LPS (1 $\mu\text{g ml}^{-1}$, 4 h) ($n=3$, mean \pm s.d.); $*P<0.0001$. The dotted line indicates that for CASP4^{KO} and CASP4^{KO}, only the Pam3CSK4 + LPS group is shown as control. **h**, TNF ELISA of SNs from Cas9^{Ctrl} and NLRP11^{KO} cells left untreated, primed with LPS (200 ng ml⁻¹, 4 h) and primed and activated with nigericin (5 μM , 30 min) ($n=3$, mean \pm s.d.); $*P<0.0001$, $**P=0.0074$. **i**, Quantitative real-time PCR (qPCR) of *IL1B* mRNA from Cas9^{Ctrl} and NLRP11^{KO} cells left untreated or primed with Pam3CSK4 (1 $\mu\text{g ml}^{-1}$, 2 h) is presented as fold change compared to control cells ($n=3$, mean \pm s.d.). **j**, IL-1 β ELISA of SN from Cas9^{Ctrl}, NLRP11^{KO} and CASP4^{KO} cells left untreated, primed with Pam3CSK4 (1 $\mu\text{g ml}^{-1}$, 2 h) and primed and transfected with poly(dA:dT) (1 $\mu\text{g ml}^{-1}$, 4 h), flagellin (0.5 $\mu\text{g ml}^{-1}$, 4 h) or FSL-1 (0.2 $\mu\text{g ml}^{-1}$, 4 h) ($n=3$, mean \pm s.d.); $*P=0.0025$; $**P<0.0001$. The dotted line indicates that for CASP4^{KO}, only the Pam3CSK4 + poly(dA:dT), flagellin and FSL-1 transfected groups are shown as control. **k**, IL-1 β and IL-6 ELISA of SN from Ctrl^{Myc} and NLRP11^{Myc} THP-1 cells left untreated, primed with LPS (200 ng ml⁻¹, 4 h) and primed and activated with nigericin (5 μM , 30 min) ($n=3$, mean \pm s.d.); $*P<0.0001$. Immunoblot of TCLs for Myc and vinculin loading control. NS, not significant.

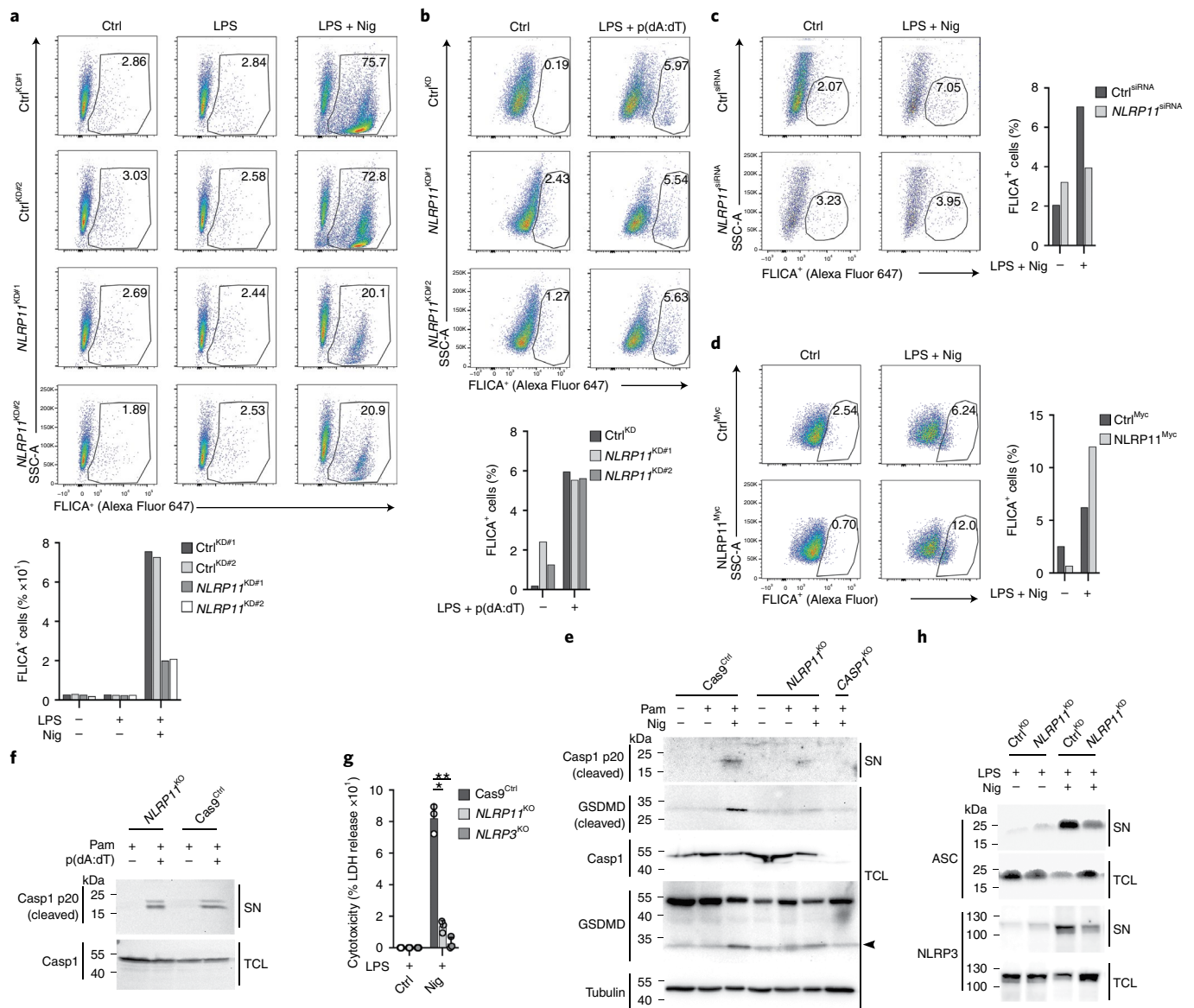


Fig. 2 | NLRP11 is required for NLRP3-mediated caspase-1 activation. **a–d**, Flow cytometry of fluorochrome-labeled inhibitors of caspases assay (FLICA) signals plotted versus side scatter area (SSC-A) in Ctrl^{KD} and NLRP11^{KD} cells (**a,b**) and primary human macrophages transfected with Ctrl^{siRNA} or NLRP11^{siRNA} (**c**) or Ctrl^{Myc} and NLRP11^{Myc} cells left untreated, primed with LPS (1 $\mu\text{g ml}^{-1}$, 1 h) and primed and activated with nigericin (5 μM , 45 min) (**a,c**), nigericin (5 μM , 15 min) (**d**) or transfected with poly(dA:dT) (6 ng ml^{-1} , 4 h) (**b**). **e**, Immunoblot for cleaved and total caspase-1, cleaved and total GSDMD and tubulin loading control from SN and TCL of Cas9^{Ctrl}, NLRP11^{KO} and CASP1^{KO} cells left untreated, primed with Pam3CSK4 (1 $\mu\text{g ml}^{-1}$, 4 h) and primed and activated with nigericin (5 μM , 30 min). The arrowhead marks the cleaved GSDMD fragment also detected by the total GSDMD antibody. **f**, Immunoblot for cleaved and total caspase-1 using SNs and TCLs of Cas9^{Ctrl} and NLRP11^{KO} cells left untreated, primed with Pam3CSK4 (1 $\mu\text{g ml}^{-1}$, 2 h) and primed + transfected with poly(dA:dT) (2 $\mu\text{g ml}^{-1}$, 6 h). **g**, LDH release from Cas9^{Ctrl}, NLRP11^{KO} and NLRP3^{KO} cells primed with LPS (200 ng ml^{-1} , 4 h) or primed and activated with nigericin (5 μM , 30 min) is presented as percent cytotoxicity compared to maximum LDH release ($n=3$, mean \pm s.d.). * $P=0.0002$, ** $P=0.0001$. **h**, Immunoblot for ASC and NLRP3 using SN and TCL of Ctrl^{KD} and NLRP11^{KD} cells primed with LPS (200 ng ml^{-1} , 4 h) or primed and activated with nigericin (5 μM , 15 min).

complex only assembled after NLRP3 inflammasome activation, which required NLRP11^{PYD}. NLRP11 was also necessary for the release of IL-1 β induced by the CAPS-associated NLRP3 mutant NLRP3^{R260V}, which placed NLRP11 at an essential step in human NLRP3 inflammasome assembly and activation. Our study therefore provides important insights into NLRP3 inflammasome regulation in human macrophages.

Results

NLRP11 is required for NLRP3-mediated cytokine release. ASC polymerization is nucleated by PYD–PYD interactions between

the inflammasome sensors and ASC^{10,11}. To identify NLRs that can nucleate ASC polymerization, we transfected NLRs into HEK293^{ASC-EGFP} cells, which stably express diffusely localized ASC-EGFP. Transfection of NLRP3 and NLRP11, but not empty plasmid (Ctrl), similarly promoted the formation of speck-like aggregates, indicating ASC polymerization (Fig. 1a). Next, we generated stable human THP-1 monocytic cells in which NLRP11 expression was knocked down (NLRP11^{KD}) with two different short hairpin RNAs (shRNAs) (Extended Data Fig. 1a) and determined the inflammasome-mediated release of IL-1 β in response to the NLRP3 activators, silica, nigericin and cholera toxin B (CTB) by

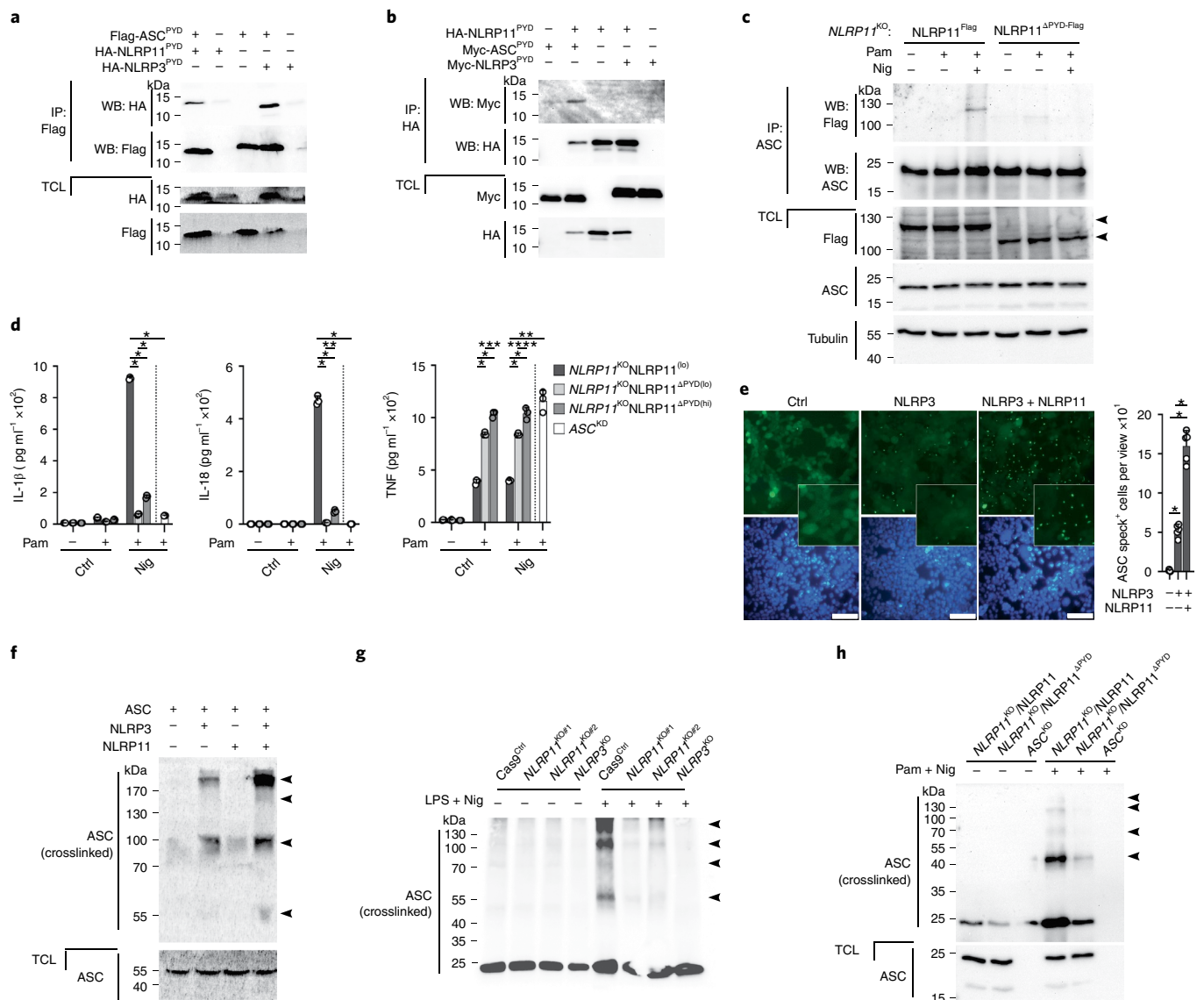


Fig. 4 | NLRP11^{PYD} recruits ASC and is necessary for efficient ASC polymerization. **a, b**, Immunoprecipitation with immobilized anti-Flag (a) and anti-HA (b) antibodies, and TCLs were analyzed by immunoblot for HA-, Myc- and Flag-tagged proteins after transient transfection of HEK293 cells with Flag-ASC^{PYD}, HA-NLRP11^{PYD} and HA-NLRP3^{PYD} (a) and HA-NLRP11^{PYD}, Myc-ASC^{PYD} and Myc-NLRP3^{PYD} (b), as indicated. **c**, Immunoprecipitation with immobilized anti-ASC antibodies from TCL of *NLRP11*^{KO} cells restored with NLRP11^{Flag} or NLRP11^{ΔPYD-Flag} left untreated, primed with Pam3CSK4 (1 μg ml⁻¹, 2 h) and primed and activated with nigericin (5 μM, 10 min); immunoprecipitates and TCLs were analyzed by immunoblot for Flag, ASC and tubulin loading control. Arrowheads indicate the correct-size protein. **d**, IL-1β, IL-18 and TNF ELISA from SNs of *NLRP11*^{KO} cells restored with low-expressing NLRP11^{Flag} cells (NLRP11^{lo}, NLRP11^{ΔPYD(lo)}), high-expressing NLRP11^{ΔPYD(hi)} and ASC^{KO} cells left untreated, primed with Pam3CSK4 (1 μg ml⁻¹, 4 h) and primed and activated with nigericin (5 μM, 25 min) ($n=3$, mean \pm s.d.); * $P < 0.0001$, ** $P = 0.0002$, *** $P = 0.0007$, **** $P = 0.0038$. The dotted line indicates that for ASC^{KO}, only the Pam3CSK4 + nigericin group is shown. **e**, Fluorescence microscopy of EGFP and DAPI in HEK293^{ASC-EGFP} cells transiently transfected with empty vector (Ctrl), NLRP3 and NLRP11 as indicated (left) and quantification of ASC speck⁺ cells per view (right). ($n=5$, mean \pm s.d.); * $P < 0.0001$, scale bars, 100 μm. **f**, immunoblot for ASC of crosslinked TCL from above cells. Arrowheads indicate oligomers. **g, h**, Immunoblot for ASC of TCLs and crosslinked TCLs from Cas9^{Ctrl}, *NLRP11*^{KO#1}, *NLRP11*^{KO#2} and *NLRP3*^{KO} cells left untreated or primed with LPS (200 ng ml⁻¹, 4 h) and activated with nigericin (5 μM, 20 min) (g) and NLRP11^{Flag}, NLRP11^{ΔPYD-Flag} and ASC^{KO} cells left untreated or primed with Pam3CSK4 (1 μg ml⁻¹, 4 h) and activated with nigericin (5 μM, 15 min) (h). Arrowheads indicate oligomers.

(LPS) directly into the cytosol of primed *NLRP11*^{KO} cells, similar to both *CASP1*^{KO} and *CASP4*^{KO} cells (Fig. 1g). Primed and nigericin-activated *NLRP11*^{KO} cells had unaltered secretion of the inflammasome-independent tumor necrosis factor (TNF) (Fig. 1h) and unaltered *IL1B* transcription (Fig. 1i) compared to Cas9^{Ctrl} cells. In agreement with reports that NLRP11 negatively regulates NF-κB signaling^{26,27}, *NLRP11*^{KO} cells showed a slight increase in TNF release compared to Cas9^{Ctrl} cells. NLRP11 selectively affected IL-1β

release by the NLRP3 inflammasome but not by AIM2, NLRC4 and NLRP7 inflammasomes, activated with poly(dA:dT), flagellin and FSL-1 transfection, respectively (Fig. 1j). *NLRP11*^{KD} also did not affect IL-1β release induced by transfection with poly(dA:dT), *Clostridium difficile* toxin B (TcdB) and FSL-1 for AIM2, pyrin and NLRP7 inflammasome activation, respectively (Extended Data Fig. 3). Furthermore, the stable expression of Myc-tagged NLRP11 in THP-1 cells (NLRP11^{Myc}) resulted in increased IL-1β release in

response to nigericin compared to Myc control (Ctrl^{Myc}) cells, without affecting the release of IL-6 (Fig. 1k). Collectively, these data strongly indicated that NLRP11 was required for NLRP3-mediated IL-1 β and IL-18 release in human macrophages.

NLRP11 is required for NLRP3-mediated caspase-1 activation. Next, we directly assessed caspase-1 activity in Ctrl^{KD} cells, which showed robust activation of caspase-1 in response to nigericin (Fig. 2a) and poly(dA:dT) (Fig. 2b), whereas *NLRP11*^{KD} cells showed markedly reduced caspase-1 activation in response to nigericin (Fig. 2a and Extended Data Fig. 4), but not to poly(dA:dT) (Fig. 2b). Nigericin-mediated caspase-1 activation was also reduced in *NLRP11*^{siRNA} transfected human macrophages compared to Ctrl^{siRNA} transfected cells (Fig. 2c), whereas nigericin-mediated caspase-1 activation was enhanced in *NLRP11*^{Myc} cells compared to Ctrl^{Myc} cells (Fig. 2d). Accordingly, the release of the cleaved, p20 form of active caspase-1 was diminished, and the subsequent proteolytic cleavage of the caspase-1 substrate GSDMD was abolished in primed *NLRP11*^{KO} cells after nigericin treatment (Fig. 2e), but not after poly(dA:dT) transfection (Fig. 2f). Pyroptosis was also defective in *NLRP11*^{KO} cells comparable to *NLRP3*^{KO} cells (Fig. 2g). Detection of ASC and NLRP3 was strongly reduced in the culture SNs of primed and nigericin-activated *NLRP11*^{KD} cells compared to Ctrl^{KD} cells but was maintained in *NLRP11*^{KD} THP-1 cell lysates (Fig. 2h), suggesting ASC and NLRP3 were retained inside the cells and not released by pyroptosis. Overall, NLRP11 regulated NLRP3-dependent caspase-1 activation, GSDMD cleavage, pyroptosis and the release of inflammasome particles.

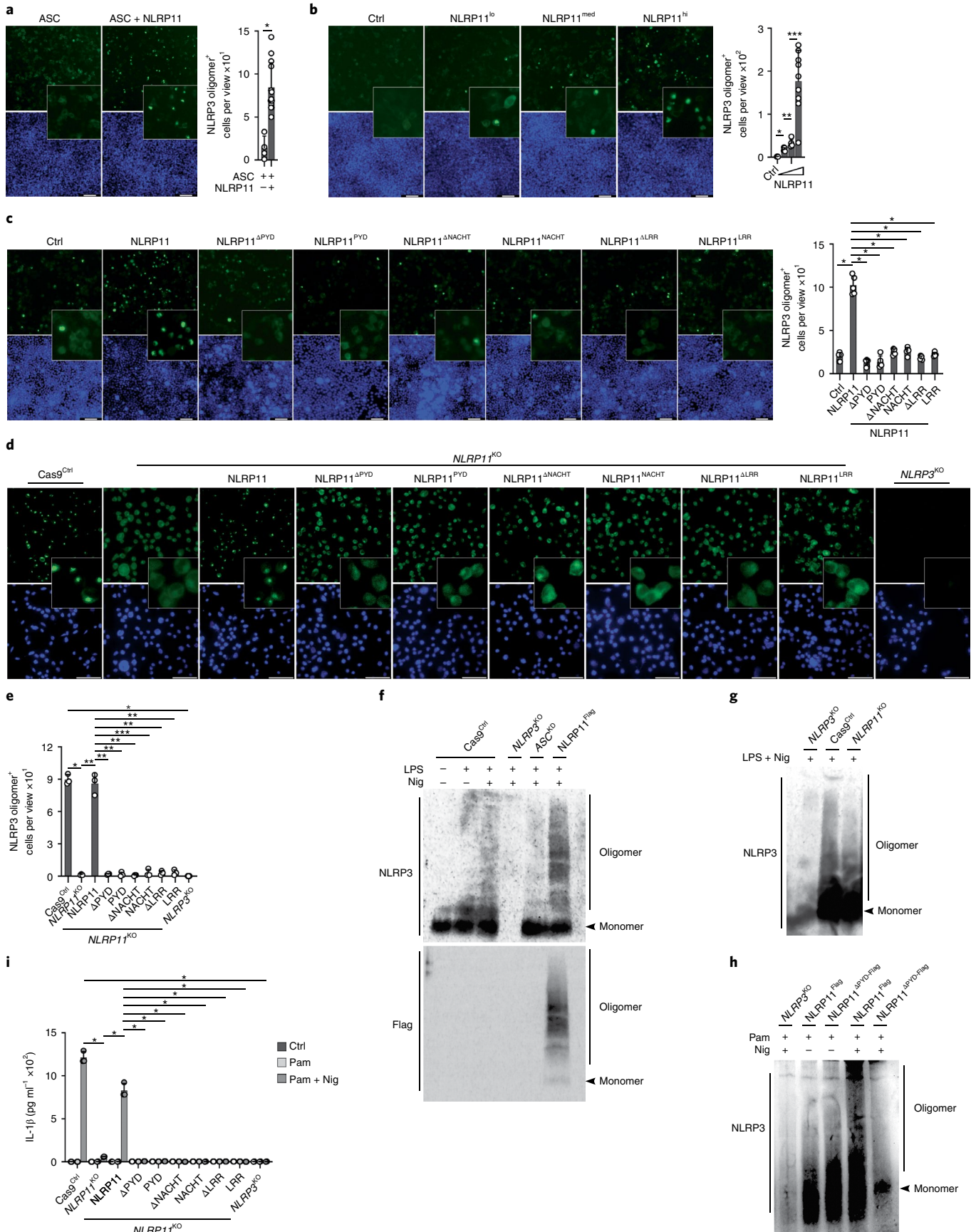
NLRP11 is a component of the NLRP3 inflammasome. To determine whether NLRP11 was a part of the NLRP3 inflammasome, we stained untreated or primed and nigericin-activated cells for NLRP11 and found redistribution of diffuse NLRP11 into characteristic 'speck'-like aggregates, which colocalized with ASC and NLRP3 upon NLRP3 activation (Fig. 3a), suggesting all three proteins formed a complex. When transiently transfected in HEK293 cells, NLRP11, ASC and NLRP3 colocalized to the characteristic ASC aggregates within concentric layers (Fig. 3b). A cross-section view indicated NLRP11 localized between the ASC core and peripheral NLRP3 (Fig. 3b), similar to the spatial organization reported for NLRP3 and NLRC4 (ref. 28). To directly test whether NLRP11 interacted with the NLRP3 inflammasome, we transduced NLRP11-Flag into *NLRP11*^{KO} cells (*NLRP11*^{Flag} cells), to allow the specific detection and selection of different levels of NLRP11 expression (Extended Data Fig. 5a). In these cells, NLRP3 copurified NLRP11^{Flag} and ASC following priming and nigericin activation, whereas NLRP3 did not bind to NLRP11^{Flag} in primed cells (Fig. 3c). To test whether NLRP11 interacted with NLRP3, ASC or both, we co-expressed NLRP11 and ASC in HEK293 cells. NLRP11 colocalized with the ASC aggregates, which are induced spontaneously after expression in HEK293 cells, in the absence of NLRP3 (Fig. 3d), suggesting that ASC could be bridging NLRP11 to the NLRP3 inflammasome. To test whether NLRP11 recruited ASC independently of NLRP3, we

immunoprecipitated ASC from primed and nigericin-activated *NLRP3*^{KO} cells expressing NLRP11^{Flag} (Extended Data Fig. 5b) and observed that ASC interacted with NLRP11^{Flag} even in the absence of NLRP3 (Fig. 3e). These data suggest that NLRP11 interacted with ASC independently of NLRP3 in response to nigericin.

ASC recruitment and polymerization requires the NLRP11^{PYD}. Both ASC and NLRP11 contain a PYD, which is known to mediate homotypic interactions. Indeed, the PYD of ASC (ASC^{PYD}) was sufficient to copurify the NLRP11^{PYD}, at levels comparable to the established ASC^{PYD}-NLRP3^{PYD} interaction (Fig. 4a). However, the NLRP11^{PYD} did not copurify the NLRP3^{PYD} (Fig. 4b). To understand the role of the NLRP11^{PYD}, we transduced *NLRP11*^{KO} cells with NLRP11 lacking the PYD (NLRP11 ^{Δ PYD-Flag}), selected for comparable expression to full-length NLRP11^{Flag} (Extended Data Fig. 5a) and immunoprecipitated ASC. Although ASC coimmunoprecipitated NLRP11^{Flag}, it did not copurify NLRP11 ^{Δ PYD-Flag} in primed and nigericin-activated cells (Fig. 4c), suggesting that the NLRP11^{PYD} was required for the NLRP11-ASC interaction. Primed and nigericin-activated NLRP11 ^{Δ PYD-Flag} cells also failed to secrete IL-1 β and IL-18 compared to NLRP11^{Flag} cells, even at increased expression of NLRP11 ^{Δ PYD-Flag} (Fig. 4d), indicating that the NLRP11^{PYD} was required for NLRP3 inflammasome-mediated cytokine release. Primed and nigericin-activated NLRP11 ^{Δ PYD-Flag} cells also showed increased secretion of TNF compared to NLRP11^{Flag} cells, comparable to ASC^{KD} cells (Fig. 4d) and reminiscent of the effect observed in *NLRP11*^{KO} cells (Fig. 1h), suggesting that the NLRP11^{PYD} was also important for this non-NLRP3 inflammasome-mediated effect on NF- κ B^{26,27}. ASC polymerization is believed to be nucleated by activated NLRP3^{10,11}. However, because NLRP11 interacted with ASC and was necessary for NLRP3 inflammasome activation, we investigated whether NLRP11 contributed to the recruitment and polymerization of ASC. In HEK293^{ASC-EGFP} cells transfected with NLRP3 at levels that promoted only limited ASC polymerization, coexpression of NLRP11 greatly enhanced ASC polymerization (Fig. 4e). Comparable results were obtained by immunoblot assays following nonreversible crosslinking of cell lysates from above cells. Expression of NLRP3 alone promoted the formation of dimeric and oligomeric ASC, whereas coexpression of NLRP3 and NLRP11 synergistically induced strong ASC polymerization (Fig. 4f). Expression of NLRP11 alone did not efficiently nucleate ASC polymerization (Fig. 4f). Primed and nigericin-activated *NLRP11*^{KO} cells (Fig. 4g) or *NLRP11*^{KD} cells (Extended Data Fig. 5c) were completely defective in ASC polymerization, similar to *NLRP3*^{KO} cells, without affecting the expression of total ASC in the cells. Only NLRP11^{Flag} cells, but not NLRP11 ^{Δ PYD-Flag} cells, promoted nigericin-induced ASC polymerization (Fig. 4h). These results indicated that NLRP3 can nucleate ASC polymerization when overexpressed but that both NLRP3 and NLRP11 are required to induce ASC polymerization in THP-1 cells in a manner dependent on the NLRP11^{PYD}.

NLRP11 is necessary for the oligomerization of human NLRP3. Next, we investigated whether NLRP11 directly contributed to NLRP3 oligomerization. Cotransfection of NLRP11 with ASC and

Fig. 5 | NLRP11 is necessary for oligomerization of human NLRP3. **a-c**, Fluorescence microscopy of EGFP and DAPI in HEK293^{NLRP3-EGFP} cells transiently cotransfected with (a) ASC and NLRP11, (b) empty plasmid (Ctrl) and increasing concentrations of NLRP11 and (c) Ctrl, NLRP11, NLRP11 ^{Δ PYD}, NLRP11 ^{Δ NACHT}, NLRP11^{NACHT}, NLRP11 ^{Δ LR} or NLRP11^{RR}, as indicated (left) and presented as NLRP3 oligomer⁺ cells per view (right) (a, ASC: $n = 4$, ASC + NLRP11: $n = 13$; b, Ctrl $n = 3$, NLRP11^{lo.med.}: $n = 5$, NLRP11^{hi.}: $n = 9$; c: $n = 5$; mean \pm s.d.; a, * $P = 0.0003$; b, * $P = 0.0006$, ** $P = 0.0164$, *** $P = 0.0009$; c, * $P < 0.0001$; a-c, scale bars, 100 μ m). **d,e**, Confocal microscopy of NLRP3 and DAPI staining, scale bars, 50 μ m (d), and quantification of NLRP3 oligomer⁺ cells per view (e) using PMA-differentiated Cas9^{Ctrl}, *NLRP3*^{KO}, *NLRP11*^{KO} and *NLRP11*^{KO} restored with NLRP11-Flag or truncated NLRP11-Flag, as indicated primed with Pam3CSK4 (1 μ g ml⁻¹, 4 h) and activated with nigericin (5 μ M, 25 min) ($n = 3$ mean \pm s.d.); * $P < 0.0001$; ** $P = 0.0001$, *** $P = 0.0002$. **f-h**, Blue native PAGE and immunoblot for NLRP3 and Flag using TCLs from Cas9^{Ctrl}, *NLRP3*^{KO}, ASC^{KD} and NLRP11^{Flag} cells (f), Cas9^{Ctrl}, *NLRP3*^{KO} and *NLRP11*^{KO} cells (g) and NLRP11^{Flag} or NLRP11 ^{Δ PYD-Flag} cells (h) left untreated, primed with LPS (200 ng ml⁻¹, 4 h) (f,g) or Pam3CSK4 (1 μ g ml⁻¹, 4 h) (h) and activated with nigericin (5 μ M, 20–30 min). **i**, IL-1 β ELISA using SNs from cells indicated above left untreated, primed with Pam3CSK4 (1 μ g ml⁻¹, 4 h) and primed and activated with nigericin (5 μ M, 25 min) ($n = 3$, mean \pm s.d.); * $P < 0.0001$.



NLRP3^{EGFP} in HEK293 cells enhanced NLRP3^{EGFP} oligomerization (Fig. 5a). Furthermore, NLRP11 cotransfection with dispersed NLRP3^{EGFP} in HEK293 cells promoted NLRP3 oligomerization in a dose-dependent manner, even in the absence of ASC, excluding any feedback from polymerized ASC (Fig. 5b), indicating that NLRP11 was necessary and sufficient to promote NLRP3 oligomerization. Because expression of NLRP11^{ΔPYD} in *NLRP11*^{KO} cells resulted in defective release of IL-1β and IL-18 (Fig. 4d), suggesting that the NLRP11^{PYD} may also be required for NLRP3 oligomerization, we tested the ability and requirement of individual NLRP11 domains to promote NLRP3 oligomerization. Comparable expression of NLRP11, but not NLRP11^{ΔPYD}, resulted in NLRP3 oligomerization in HEK293 cells (Fig. 5c and Extended Data Fig. 6a). The PYD, NACHT or LRR alone did not support NLRP3 oligomerization (Fig. 5c). NLRP11 lacking the NACHT domain (NLRP11^{ΔNACHT}) or the LRR (NLRP11^{ΔLRR}) was also defective in inducing NLRP3 oligomerization (Fig. 5c), suggesting that intact NLRP11 was required. To further interrogate this mechanism, we stably restored the expression of NLRP11, NLRP11^{ΔPYD}, NLRP11^{ΔNACHT}, NLRP11^{ΔLRR}, NLRP11^{PYD}, NLRP11^{NACHT} and NLRP11^{LRR} in *NLRP11*^{KO} cells and sorted cells for comparable expression (Extended Data Fig. 6b). Primed and nigericin-activated Cas9^{Ctrl} and *NLRP11*^{KO} cells expressing NLRP11, but not *NLRP11*^{KO} cells or *NLRP11*^{KO} cells expressing any of the other truncated NLRP11 proteins, induced NLRP3 oligomerization, as determined by microscopy and quantification of NLRP3 oligomers using NLRP3^{KO} cells as a specificity control (Fig. 5d,e). Biochemical analysis using blue native gel electrophoresis also demonstrated the nigericin-induced NLRP3 oligomerization in primed Cas9^{Ctrl} cells, which was further enhanced in NLRP11^{Flag} cells (Fig. 5f) but reduced in *NLRP11*^{KO} cells (Fig. 5g) or NLRP11^{ΔPYD-Flag} cells (Fig. 5h). NLRP3^{KO} cells were used as a specificity control. This analysis also revealed the oligomerization of NLRP11 itself in primed and nigericin-activated NLRP11^{Flag} cells (Fig. 5f). Primed and nigericin-activated NLRP11^{Flag} cells, but not *NLRP11*^{KO} cells and *NLRP11*^{KO} cells expressing any truncated NLRP11, secreted IL-1β comparable to Cas9^{Ctrl} cells (Fig. 5i). Collectively, these results demonstrated that intact NLRP11 was necessary for the oligomerization of NLRP3.

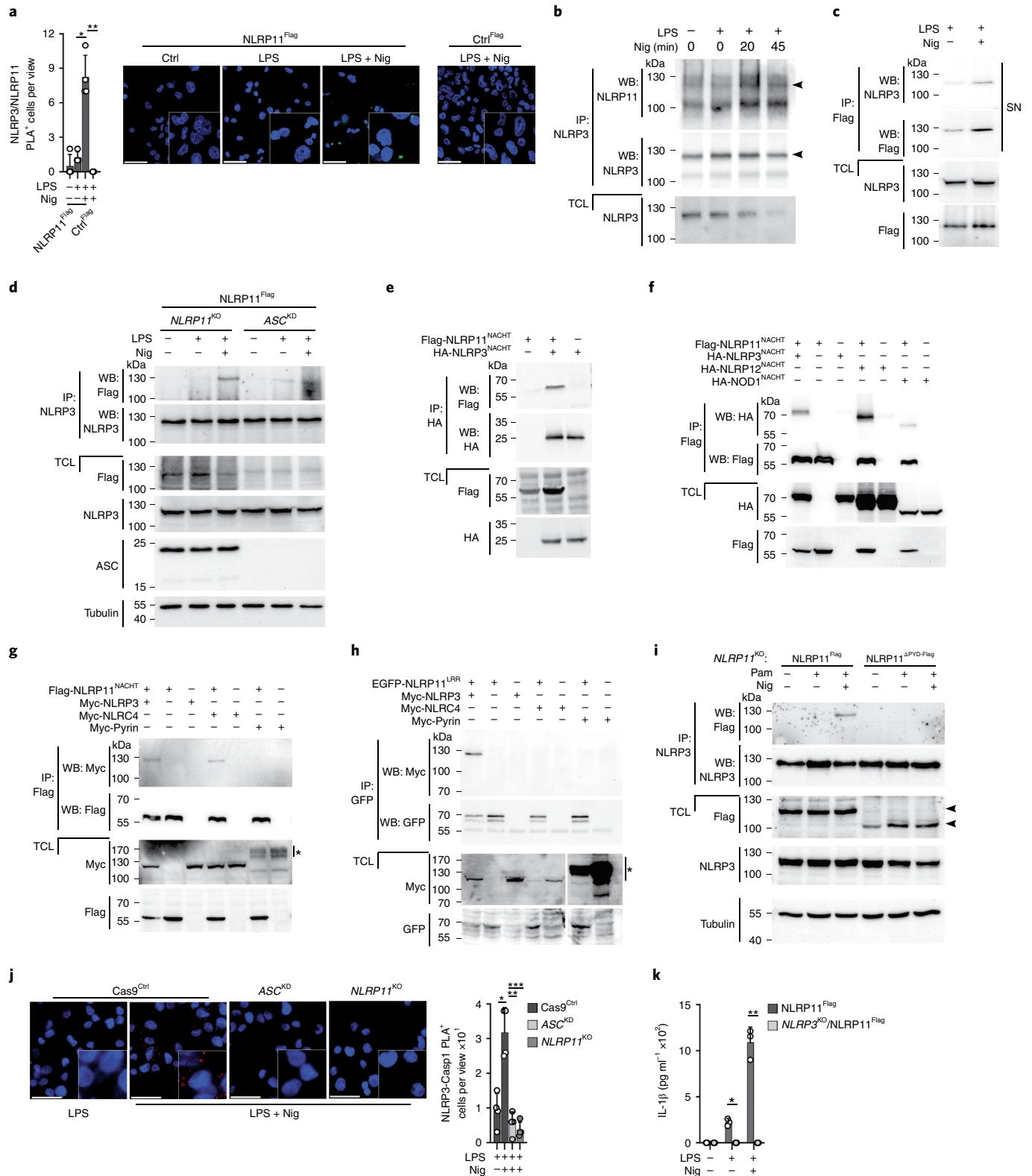
NLRP11 promotes NLRP3 inflammasome assembly. Next, we investigated whether NLRP11 interacted with NLRP3 using a proximity ligation assay (PLA). A specific PLA signal was detected in primed and nigericin-activated NLRP11^{Flag} cells, but not in primed cells (Fig. 6a). NLRP3 immunoprecipitation further corroborated the nigericin-dependent interaction of NLRP3 with endogenous

NLRP11 in THP-1 cells (Fig. 6b). The reduced expression of NLRP3 and NLRP11 in TCL after prolonged activation (45 min) was likely the result of partially released NLRP3 inflammasome components (Fig. 6b). Accordingly, Flag immunoprecipitation from the SNs of primed and nigericin-activated, but not from primed, NLRP11^{Flag} cells copurified NLRP3 (Fig. 6c), indicating that NLRP11 and NLRP3 were released as a complex by pyroptosis. To determine whether the NLRP3–NLRP11 interaction occurred independently of ASC, we expressed NLRP11^{Flag} in ASC^{KD} cells (Extended Data Fig. 5b) and immunoprecipitated NLRP3. NLRP3 coimmunoprecipitated NLRP11 in primed and nigericin-activated NLRP11^{Flag} cells, and this interaction was also observed in ASC^{KD} cells expressing NLRP11^{Flag} (Fig. 6d), suggesting that NLRP11 interacted with NLRP3 independently of ASC. NLRP3 oligomerization is mediated by the NACHT domain⁸. In HEK293 cells, the NLRP11^{NACHT} bound directly to the NLRP3^{NACHT}, as demonstrated by coimmunoprecipitation of transiently transfected NLRP11^{NACHT} and NLRP3^{NACHT} domains (Fig. 6e), but the NLRP11^{NACHT} also bound to the NLRP12^{NACHT} and NOD1^{NACHT} domains (Fig. 6f). Binding was still observed under very stringent conditions in RIPA buffer (Extended Data Fig. 7a) and in buffers with up to 800 mM NaCl (Extended Data Fig. 7b), indicating that the NLRP11^{NACHT} bound with high affinity to other NACHT domains. To address whether isolated NACHT domains were more easily accessible for interactions in the absence of intramolecular interactions with the LRR and/or the PYD in the intact protein^{9,29}, we tested the interaction of the NLRP11^{NACHT} with full-length NLRP3 and NLRC4 by transient transfection of HEK293 cells. The NLRP11^{NACHT} coimmunoprecipitated NLRP3 and NLRC4 (Fig. 6g), even though the NLRC4 inflammasome was not affected by NLRP11 (Fig. 1j), confirming previous reports of spontaneous interactions between NLR NACHT domains in HEK293 cells³⁰. The NLRP11^{NACHT} did not interact with pyrin, which lacks a NACHT domain (Fig. 6g). These results suggested that although the NLRP11^{NACHT} can interact with the NLRP3^{NACHT}, additional events may facilitate and determine the specificity of these interactions in macrophages. NEK7 promotes NLRP3 oligomerization and ASC polymerization but cannot mediate NLRP3 activation on its own^{20–22}. NEK7 binds to the LRR and NACHT domains of NLRP3 to bridge two adjacent NLRP3 molecules²³. NEK7 interacted with NLRP3 in LPS-primed and LPS-primed and nigericin-activated Cas9^{Ctrl} and *NLRP11*^{KO} cells (Extended Data Fig. 7c), indicating that NLRP11 does not mediate the NEK7–NLRP3 interaction. We did not observe substantial NLRP3 localization to the mitochondria in untreated, primed and primed and nigericin-activated Cas9^{Ctrl} and *NLRP11*^{KO} cells (Extended Data Fig. 8a), but, as previously

Fig. 6 | NLRP11 acts as a scaffold for NLRP3 inflammasome assembly. **a**, Confocal microscopy of PLA (green) between NLRP3 and Flag and DAPI using PMA-differentiated Ctrl^{Flag} and NLRP11^{Flag} cells left untreated, primed with LPS (200 ng ml⁻¹, 4 h) and primed and activated with nigericin (5 μM, 20 min); scale bar, 50 μm; (right), and quantification of PLA⁺ cells per view (left) ($n=4$, mean \pm s.d.); * $P=0.0004$; ** $P=0.0001$. **b**, Immunoprecipitation with immobilized anti-NLRP3 antibodies using TCLs from untreated, LPS-primed (200 ng ml⁻¹, 4 h) and primed + nigericin (5 μM, 20 min and 45 min) activated THP-1 cells and immunoblot of immunoprecipitates and TCLs for NLRP11 and NLRP3. Arrowheads indicate the correct-size proteins. **c**, Immunoprecipitation with immobilized anti-Flag antibodies using SNs of NLRP11^{Flag} cells primed with LPS (200 ng ml⁻¹, 4 h) and primed and activated with nigericin (5 μM, 10 min) and immunoblot of immunoprecipitates and TCLs for NLRP3 and Flag. **d**, Immunoprecipitation with immobilized anti-NLRP3 antibodies using TCLs from *NLRP11*^{KO} and ASC^{KD} THP-1 cells restored with NLRP11-Flag left untreated, LPS-primed (200 ng ml⁻¹, 2 h) and primed and activated with nigericin (5 μM, 10 min), and immunoblot of immunoprecipitates and TCLs by immunoblot for Flag, NLRP3, ASC and tubulin loading control. **e–h**, Immunoprecipitation with immobilized anti-HA (e), anti-Flag (f,g) and anti-EGFP (h) antibodies using TCLs from HEK293 cells transiently transfected with Flag-NLRP11^{NACHT} and HA-NLRP3^{NACHT} (e); Flag-NLRP11^{NACHT}, HA-NLRP3^{NACHT}, HA-NLRP12^{NACHT} and HA-NOD1^{NACHT} (f); Flag-NLRP11^{NACHT}, Myc-NLRP3, Myc-NLRC4 and Myc-pyrin (g); and EGFP-NLRP11^{LRR}, Myc-NLRP3, Myc-NLRC4 and Myc-pyrin as indicated (h); and immunoblot of immunoprecipitates and TCLs for HA-, Flag-, Myc- and EGFP. Asterisk denotes modified pyrin (g,h). The gap in the TCLs in panel h marks an empty lane between NLRC4 and pyrin. **i**, Immunoprecipitation with immobilized anti-NLRP3 antibodies using TCLs from NLRP11^{Flag} and NLRP11^{ΔPYD-Flag} cells left untreated, primed with Pam3CSK4 (1 μg ml⁻¹, 2 h) and primed and activated with nigericin (5 μM, 10 min) and immunoblot of immunoprecipitates and TCLs for Flag, NLRP3 and tubulin loading control. **j**, Confocal microscopy of PLA (red) between NLRP3 and caspase-1 and DAPI of PMA-differentiated Cas9^{Ctrl}, ASC^{KD} and *NLRP11*^{KO} cells primed with LPS (200 ng ml⁻¹, 4 h) and primed and activated with nigericin (5 μM, 20 min); scale bar, 50 μm; (left), and quantification of PLA⁺ cells per view (right) ($n=4$, mean \pm s.d.); * $P=0.0021$; ** $P=0.0006$, *** $P=0.0003$. **k**, IL-1β ELISA of SNs from Cas9^{Ctrl} and *NLRP3*^{KO} cells stably expressing NLRP11-Flag left untreated, primed with LPS (200 ng ml⁻¹, 4 h) and primed and activated with nigericin (5 μM, 30 min) ($n=3$, mean \pm s.d.); * $P=0.0006$, ** $P=0.0003$.

described³¹, NLRP3-activating stimuli caused the disassembly of the trans-Golgi network (TGN), and NLRP3 localization to the dispersed TGN in Cas9^{Ctrl} cells and also in *NLRP11*^{KO} cells (Extended Data Fig. 8b), indicating that NLRP11 did not affect the intracellular localization of NLRP3. Because the LRR has a key role in assembling mouse NLRP3 oligomers³², we tested whether the NLRP11^{LRR} was involved in the NLRP3–NLRP11 interaction. Transient transfection

of HEK293 cells with NLRP11^{LRR} and NLRP3, NLRC4 (which has a LRR) or pyrin (which lacks a LRR) demonstrated that the NLRP11^{LRR} coprecipitated NLRP3, but not NLRC4 or pyrin (Fig. 6h). NLRP3 coimmunoprecipitated NLRP11 in primed and nigericin-activated NLRP11^{Flag} cells, but not in NLRP11^{ΔPYD-Flag} cells (Fig. 6i). To test whether NLRP11 directly controlled the assembly of the NLRP3 inflammasome, we performed a PLA between NLRP3



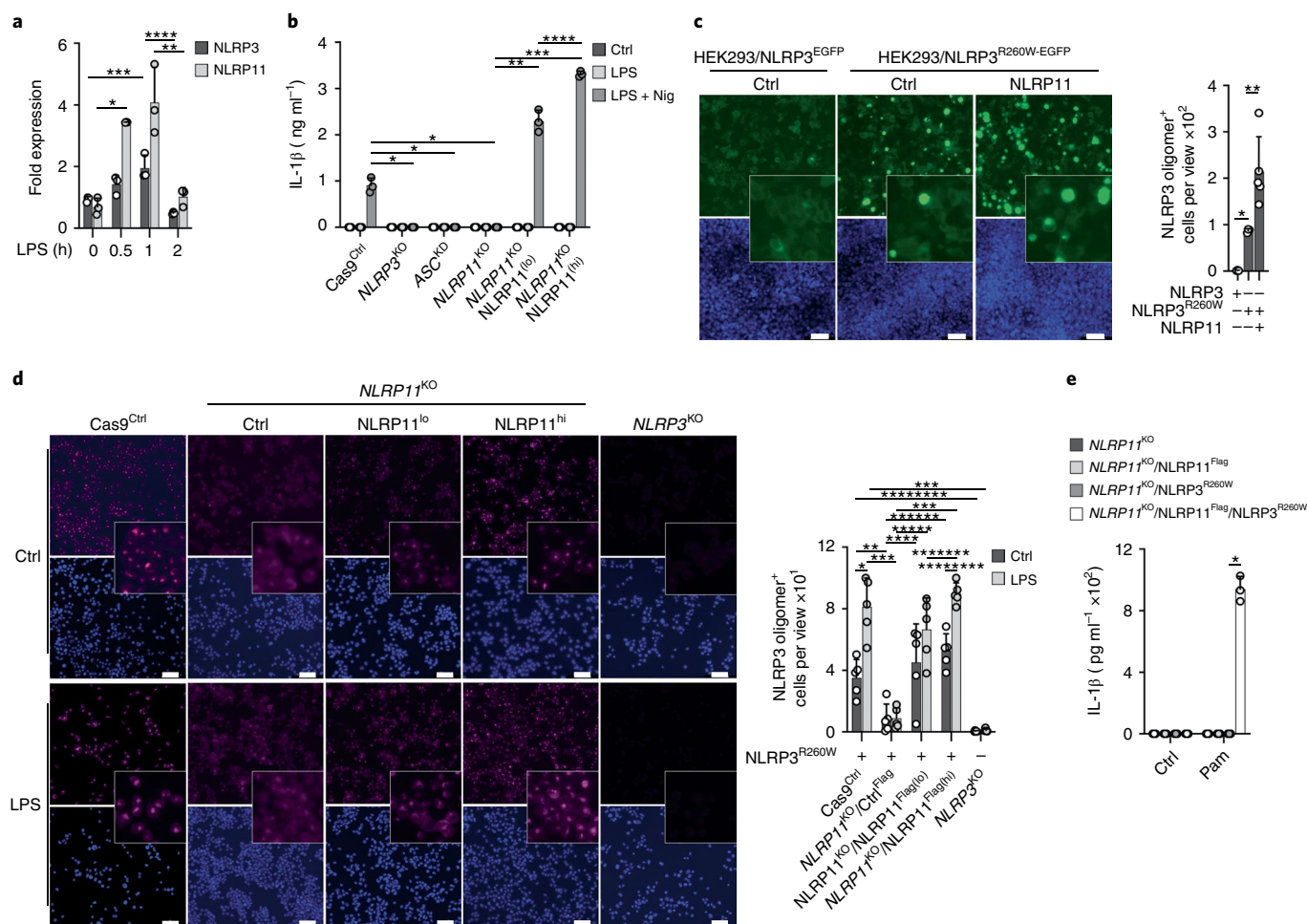


Fig. 7 | NLRP11 is necessary for IL-1 β release in CAPS. **a**, qPCR of *NLRP3* and *NLRP11* mRNA levels from THP-1 cells primed with LPS (200 ng ml⁻¹) as indicated, presented as fold expression to average mRNA levels present in uninduced cells ($n=3$, mean \pm s.d.); * $P < 0.0001$, *** $P = 0.0103$, **** $P = 0.0145$, ***** $P = 0.0037$. **b**, IL-1 β ELISA of SN from Cas9^{Ctrl}, *NLRP11*^{KO}, *NLRP3*^{KO}, ASC^{KD}, *NLRP11*^{Flag(lo)} and *NLRP11*^{Flag(hi)} cells primed with LPS (200 ng ml⁻¹, 4 h) and primed and activated with nigericin (5 μ M, 30 min) ($n=3$, mean \pm s.d.); * $P = 0.0006$; ** $P = 0.0012$, *** $P < 0.0001$, **** $P = 0.0021$. **c**, Fluorescence microscopy of EGFP and DAPI in HEK293^{NLRP3-EGFP} and HEK293^{NLRP3R260W-EGFP} cells transiently cotransfected with empty vector (Ctrl) or NLRP11; scale bars, 100 μ m (left), and quantification of NLRP3 oligomer⁺ cells per view (right) (Ctrl: $n=5$, mean \pm s.d.); * $P < 0.0001$; ** $P = 0.029$. **d**, Confocal microscopy of DAPI and NLRP3 immunostained PMA-differentiated Cas9^{Ctrl}, *NLRP11*^{KO}, *NLRP11*^{Flag(lo)} and *NLRP11*^{Flag(hi)} and *NLRP3*^{KO} cells stably expressing NLRP3^{R260W} left untreated (Ctrl) or primed with LPS (200 ng ml⁻¹, 4 h); scale bars, 50 μ m (left), and quantification of NLRP3 oligomer⁺ cells per view (right) ($n=5$, mean \pm s.d.); * $P = 0.0017$; ** $P = 0.0046$, *** $P < 0.0001$, **** $P = 0.0153$, ***** $P = 0.0003$, *****($P = 0.0001$, *****($P = 0.0427$, *****($P = 0.0002$. **e**, IL-1 β ELISA of SNs from *NLRP11*^{KO} and *NLRP11*^{Flag} cells stably expressing NLRP3^{R260W} left untreated (Ctrl) or primed with Pam3CSK4 (1 μ g ml⁻¹, 2 h) ($n=3$, mean \pm s.d.). * $P < 0.0001$.

and caspase-1. A positive PLA signal was detected in primed and nigericin-activated Cas9^{Ctrl} cells, but not in *NLRP11*^{KO} or ASC^{KD} cells (Fig. 6j). However, expression of NLRP11 cannot compensate for the loss of NLRP3, as NLRP11 overexpression could not induce IL-1 β release in primed and nigericin-activated *NLRP3*^{KO} cells (Fig. 6k). Collectively, these results showed that NLRP11 interacts with NLRP3 independently of ASC through its NACHT and LRRs, but an intact NLRP11, including the NLRP11^{PYD}, was nevertheless required for promoting nigericin-induced interactions between NLRP11 and NLRP3.

NLRP11 is necessary for IL-1 β release in CAPS. qPCR analysis indicated that *NLRP11* mRNA was induced in primed THP-1 cells, similar to the inducible expression of *NLRP3* (Fig. 7a). In primed *NLRP11*^{KO} cells restored with low or high amounts of NLRP11 protein to mimic the inducible expression of NLRP11-primed cells (Fig. 7b), we observed an NLRP11 concentration-dependent increase in

IL-1 β secretion in response to nigericin treatment (Fig. 7c), indicating that the activation of the NLRP3 inflammasome was influenced by the amount of NLRP11. In patients with CAPS, myeloid-lineage restricted mutations in NLRP3 and somatic mosaicism⁶ allow NLRP3 activation in the absence of an activation signal, and priming alone is sufficient to trigger NLRP3 inflammasome-mediated IL-1 β release³³. The majority of CAPS mutations are localized within the NACHT domain and prevent the autoinhibited conformation of NLRP3 (ref. 34). Accordingly, stable expression of the CAPS mutation NLRP3^{R260W-EGFP} in HEK293 cells resulted in spontaneous oligomerization of NLRP3 (Fig. 7d), whereas wild-type NLRP3^{EGFP} was distributed diffusely throughout the cells (Fig. 7d). Coexpression of NLRP11 in HEK293 cells further increased the aggregation of NLRP3^{R260W-EGFP} (Fig. 7d), indicating that NLRP11 even enhanced the oligomerization of the constitutively active NLRP3^{R260W}. Stable expression of NLRP3^{R260W} also resulted in spontaneous oligomerization of NLRP3^{R260W} in Cas9^{Ctrl} cells when immunostained for NLRP3

(Fig. 7e), but not in *NLRP11*^{KO} cells (Fig. 7e), whereas stable reexpression of NLRP11^{Flag} in *NLRP11*^{KO} cells restored NLRP3^{R260W} oligomerization in a dose-dependent manner (Fig. 7e). Priming further increased the number of NLRP3^{R260W} oligomers in Cas9^{Ctrl} cells, but not in *NLRP11*^{KO} cells (Fig. 7e). IL-1 β was already released in primed NLRP11^{Flag} cells, but not in *NLRP11*^{KO} cells expressing NLRP3^{R260W} (Fig. 7f). These results indicated that NLRP11 was also necessary for facilitating oligomerization and promoting IL-1 β release from mutant NLRP3 that causes CAPS. Therefore, NLRP11 is an essential component of the NLRP3 inflammasome (Extended Data Fig. 9).

Discussion

Here, we identified NLRP11 as an essential component of the NLRP3 inflammasome in human macrophages, which was required for caspase-1 activation, release of IL-1 β and IL-18 and pyroptosis. NLRP11 bound to ASC through homotypic PYD–PYD interactions, which was required for nigericin-induced ASC polymerization. NLRP11 also independently interacted with NLRP3, which involved the NLRP11^{LRR} and the NLRP11^{NACHT} domains and facilitated NLRP3 oligomerization.

The NLRP11^{NACHT} did not specifically interact with NLRP3 in HEK293 cells. This unspecific affinity of NACHT domains when expressed in HEK293 cells has been reported earlier³⁰. In THP-1 cells, the interaction between NLRP11 and NLRP3 occurred after NLRP3 activation. Therefore, we speculate that in macrophages additional unknown signals may be required to confer specificity to NLRP11^{NACHT} domain interactions. Additional specificity is provided by the NLRP11^{LRR}, which interacted with NLRP3, but not with NLRC4. Taken together, it is very likely that the NLRP11^{LRR} and the NLRP11^{NACHT} domains both contributed to the specific interaction between NLRP3 and NLRP11, reminiscent of the interaction between NLRP3 and NEK7 (ref. 23). Other NACHT domain-mediated NLR hetero-oligomerizations have been described, including NLRC4–NLRP3 (refs. 28,35), NAIP–NLRC4 (refs. 36,37) and Nod2–NLRP1 (ref. 38). NLRC5 also interacts with the NLRP3^{NACHT} to regulate NLRP3 by an unknown mechanism³⁹ but has more recently been linked to major histocompatibility complex class I transactivation^{40,41}. Even though NLRP11 and NLRP3 did not interact through their PYDs, the NLRP11^{PYD} was still crucial for complex formation, because deletion of the PYD prevented NLRP11 recruitment to the NLRP3 inflammasome, NLRP3 oligomerization and NLRP3 inflammasome responses, which required an intact NLRP11 protein. NLRP3 can nucleate ASC polymerization *in vitro*, and we observed this ability in HEK293 cells, but only if NLRP3 was overexpressed. Increasing the expression of NLRP3 during inflammasome priming contributes to, but is not sufficient for, inflammasome activation^{3–5}. Low-level expression of NLRP3 did not nucleate ASC polymerization in HEK293 cells, and even priming-induced elevation of NLRP3 expression was insufficient in THP-1 cells in the absence of NLRP11. NLRP11 was required for NLRP3 inflammasome responses in a dose-dependent manner, but NLRP11 expression was not able to compensate for the loss of NLRP3, indicating that NLRP11 alone could not assemble an inflammasome under these conditions. This mode of activation is unique, because NLRP11 interacted with NLRP3 as well as ASC, and all three were required for NLRP3 inflammasome assembly in THP-1 cells. Other described mechanisms for inflammasome activation require bridging of the NLRP3–ASC interaction by GBP5²⁴, or bridging NLRP3 molecules through NACHT–LRR interaction by NEK7 (ref. 23). NLRP11 uniquely combines these mechanisms. NLRP11 was required for the response to all tested soluble and crystalline NLRP3 triggers, supporting its essential role within the NLRP3 inflammasome.

NLRP11 is encoded in humans and absent from mice⁴², but whether this mechanism is unique to human macrophages will require additional studies. Nevertheless, several other examples exist for increased complexity of inflammasome regulation in

humans, including the family of PYD- and CARD-only proteins⁴³. In addition to its function in NLRP3 inflammasome activation, NLRP11 could potentially function as an inflammasome sensor. Arguably, this would require the ability of NLRP11 to nucleate ASC polymerization, and based on our ASC^{EGFP} polymerization assays in HEK293 cells, some NLRP11-mediated ASC polymerization was possible, especially in cells with sufficiently high NLRP11 expression. However, expression of NLRP11 in THP-1 cells failed to polymerize ASC in the absence of activated NLRP3, suggesting that physiological amounts of NLRP3 require the cooperation between NLRP3 and NLRP11, even though macrophages are the cells with the highest expression of NLRP3 (ref. 44).

Little is known about NLRP11, and there are conflicting reports on its role in type I interferon (IFN) or NF- κ B signaling^{26,27,45}. NLRP11 causes degradation of TRAF6 to inhibit TLR-mediated NF- κ B activation²⁷, and we observed slightly elevated TNF release in *NLRP11*^{KO} cells. However, NF- κ B-dependent IL-6 release and *IL1B* transcription were not impacted. NLRP11 also binds to DDX3X and inhibits IFN- β and reduces caspase-1 activity in HEK293T cells⁴⁶. siRNA-mediated silencing of NLRP11 in THP-1 cells slightly elevates Sendai virus-induced IFN- β production and does not affect IL-1 β release⁴⁵, but Sendai virus already completely prevents NLRP3 inflammasome assembly⁴⁷. Several other NLRs, including NLRP2, NLRP3, NLRP6, NLRP7, NLRP12 and NLRC5, have been linked to inflammasomes, as well as transcriptional responses through regulating NF- κ B, mitogen-activated protein kinase and IFN signaling⁴⁸. Overall, our identification of NLRP11 as an essential adaptor or scaffold for NLRP3 inflammasome assembly and activation provides important insights into the still incompletely understood NLRP3 inflammasome response in humans. NLRP3 is uniquely positioned as a central sensor for infections and cellular stress and has been implicated in a wide range of inflammatory diseases ranging from crystal arthropathies to hereditary autoinflammatory disorders⁴⁹. NLRP11 may provide an important checkpoint control for NLRP3 inflammasome assembly. Intriguingly, NLRP11 is also necessary for NLRP3 inflammasome responses initiated by CAPS-linked NLRP3 mutations, which may have important clinical implications.

Online content

Any methods, additional references, Nature Research reporting summaries, source data, extended data, supplementary information, acknowledgements, peer review information; details of author contributions and competing interests; and statements of data and code availability are available at <https://doi.org/10.1038/s41590-022-01220-3>.

Received: 29 April 2021; Accepted: 19 April 2022;

Published online: 27 May 2022

References

- Martinon, F., Burns, K. & Tschopp, J. The inflammasome: a molecular platform triggering activation of inflammatory caspases and processing of proIL- β . *Mol. Cell* **10**, 417–426 (2002).
- Kesavardhana, S., Malireddi, R. K. S. & Kanneganti, T. D. Caspases in cell death, inflammation, and pyroptosis. *Annu. Rev. Immunol.* **38**, 567–595 (2020).
- Swanson, K. V., Deng, M. & Ting, J. P. The NLRP3 inflammasome: molecular activation and regulation to therapeutics. *Nat. Rev. Immunol.* **19**, 477–489 (2019).
- Kelley, N. et al. The NLRP3 inflammasome: an overview of mechanisms of activation and regulation. *Int. J. Mol. Sci.* **20**, 3328 (2019).
- Moretti, J. & Blander, J. Increasing complexity of NLRP3 inflammasome regulation. *J. Leukoc. Biol.* **109**, 561–571 (2020).
- Booshehri, L. M. & Hoffman, H. M. CAPS and NLRP3. *J. Clin. Immunol.* **39**, 277–286 (2019).
- Hoffman, H. M., Mueller, J. L., Broide, D. H., Wanderer, A. A. & Kolodner, R. D. Mutation of a new gene encoding a putative pyrin-like protein causes familial cold autoinflammatory syndrome and Muckle-Wells syndrome. *Nat. Genet.* **29**, 301–305 (2001).

8. Duncan, J. A. et al. Cryopyrin/NALP3 binds ATP/dATP, is an ATPase, and requires ATP binding to mediate inflammatory signaling. *Proc. Natl Acad. Sci. U S A* **104**, 8041–8046 (2007).
9. Hafner-Bratkovic, I. et al. NLRP3 lacking the leucine-rich repeat domain can be fully activated via the canonical inflammasome pathway. *Nat. Commun.* **9**, 5182 (2018).
10. Cai, X. et al. Prion-like polymerization underlies signal transduction in antiviral immune defense and inflammasome activation. *Cell* **156**, 1207–1222 (2014).
11. Lu, A. et al. Unified polymerization mechanism for the assembly of ASC-dependent inflammasomes. *Cell* **156**, 1193–1206 (2014).
12. Dick, M. S., Sborgi, L., Ruhl, S., Hiller, S. & Broz, P. ASC filament formation serves as a signal amplification mechanism for inflammasomes. *Nat. Commun.* **7**, 11929 (2016).
13. Bryan, N. B., Dorfleutner, A., Rojanasakul, Y. & Stehlik, C. Activation of inflammasomes requires intracellular redistribution of the apoptotic speck-like protein containing a caspase recruitment domain. *J. Immunol.* **182**, 3173–3182 (2009).
14. Fernandes-Alnemri, T. et al. The pyroptosome: a supramolecular assembly of ASC dimers mediating inflammatory cell death via caspase-1 activation. *Cell Death Differ.* **14**, 1590–1604 (2007).
15. Elliott, J. M., Rouge, L., Wiesmann, C. & Scheer, J. M. Crystal structure of procaspase-1 zymogen domain reveals insight into inflammatory caspase autoactivation. *J. Biol. Chem.* **284**, 6546–6553 (2009).
16. He, W. T. et al. Gasdermin D is an executor of pyroptosis and required for interleukin-1 β secretion. *Cell Res.* **25**, 1285–1298 (2015).
17. Kayagaki, N. et al. Caspase-11 cleaves gasdermin D for non-canonical inflammasome signalling. *Nature* **526**, 666–671 (2015).
18. Shi, J. et al. Cleavage of GSDMD by inflammatory caspases determines pyroptotic cell death. *Nature* **526**, 660–665 (2015).
19. Munoz-Planillo, R. et al. K(+) efflux is the common trigger of NLRP3 inflammasome activation by bacterial toxins and particulate matter. *Immunity* **38**, 1142–1153 (2013).
20. He, Y., Zeng, M. Y., Yang, D., Motro, B. & Nunez, G. NEK7 is an essential mediator of NLRP3 activation downstream of potassium efflux. *Nature* **530**, 354–357 (2016).
21. Schmid-Burgk, J. L. et al. A genome-wide CRISPR (clustered regularly interspaced short palindromic repeats) screen identifies NEK7 as an essential component of NLRP3 inflammasome activation. *J. Biol. Chem.* **291**, 103–109 (2016).
22. Shi, H. et al. NLRP3 activation and mitosis are mutually exclusive events coordinated by NEK7, a new inflammasome component. *Nat. Immunol.* **17**, 250–258 (2016).
23. Sharif, H. et al. Structural mechanism for NEK7-licensed activation of NLRP3 inflammasome. *Nature* **570**, 338–343 (2019).
24. Shenoy, A. R. et al. GBP5 promotes NLRP3 inflammasome assembly and immunity in mammals. *Science* **336**, 481–485 (2012).
25. Chu, L. H. et al. The oxidized phospholipid oxPAPC protects from septic shock by targeting the non-canonical inflammasome in macrophages. *Nat. Commun.* **9**, 996 (2018).
26. Ellwanger, K. et al. The NLR family pyrin domain-containing 11 protein contributes to the regulation of inflammatory signaling. *J. Biol. Chem.* **293**, 2701–2710 (2018).
27. Wu, C. et al. NLRP11 attenuates Toll-like receptor signalling by targeting TRAF6 for degradation via the ubiquitin ligase RNF19A. *Nat. Commun.* **8**, 1977 (2017).
28. Man, S. M. et al. Inflammasome activation causes dual recruitment of NLRC4 and NLRP3 to the same macromolecular complex. *Proc. Natl Acad. Sci. U S A* **111**, 7403–7408 (2014).
29. Hu, Z. et al. Crystal structure of NLRC4 reveals its autoinhibition mechanism. *Science* **341**, 172–175 (2013).
30. Damiano, J. S., Oliveira, V., Welsh, K. & Reed, J. C. Heterotypic interactions among NACHT domains: implications for regulation of innate immune responses. *Biochem J.* **381**, 213–219 (2004).
31. Chen, J. & Chen, Z. J. PtdIns4P on dispersed trans-Golgi network mediates NLRP3 inflammasome activation. *Nature* **564**, 71–76 (2018).
32. & Andreeva, L. et al. NLRP3 cages revealed by full-length mouse NLRP3 structure control pathway activation. *Cell* **184**, 6299–6312 (2021).
33. Agostini, L. et al. NALP3 forms an IL-1 β -processing inflammasome with increased activity in Muckle-Wells autoinflammatory disorder. *Immunity* **20**, 319–325 (2004).
34. Tapia-Abellan, A. et al. MCC950 closes the active conformation of NLRP3 to an inactive state. *Nat. Chem. Biol.* **15**, 560–564 (2019).
35. Qu, Y. et al. NLRP3 recruitment by NLRC4 during Salmonella infection. *J. Exp. Med.* **213**, 877–885 (2016).
36. Hu, Z. et al. Structural and biochemical basis for induced self-propagation of NLRC4. *Science* **350**, 399–404 (2015).
37. Zhang, L. et al. Cryo-EM structure of the activated NAIP2-NLRC4 inflammasome reveals nucleated polymerization. *Science* **350**, 404–409 (2015).
38. Hsu, L. C. et al. A NOD2-NALP1 complex mediates caspase-1-dependent IL-1 β secretion in response to Bacillus anthracis infection and muramyl dipeptide. *Proc. Natl Acad. Sci. U S A* **105**, 7803–7808 (2008).
39. Davis, B. K. et al. Cutting edge: NLRC5-dependent activation of the inflammasome. *J. Immunol.* **186**, 1333–1337 (2011).
40. Meissner, T. B., Li, A. & Kobayashi, K. S. NLRC5: a newly discovered MHC class I transactivator (CITA). *Microbes Infect.* **14**, 477–484 (2012).
41. Staehli, F. et al. NLRC5 deficiency selectively impairs MHC class I-dependent lymphocyte killing by cytotoxic T cells. *J. Immunol.* **188**, 3820–3828 (2012).
42. Reed, J. C. et al. Comparative analysis of apoptosis and inflammation genes of mice and humans. *Genome Res.* **13**, 1376–1388 (2003).
43. Stehlik, C. & Dorfleutner, A. COPs and POPs: modulators of inflammasome activity. *J. Immunol.* **179**, 7993–7998 (2007).
44. Uhlen, M. et al. Proteomics. Tissue-based map of the human proteome. *Science* **347**, 1260419 (2015).
45. Qin, Y. et al. NLRP11 disrupts MAVS signalosome to inhibit type I interferon signaling and virus-induced apoptosis. *EMBO Rep.* **18**, 2160–2171 (2017).
46. Kienes, I. et al. DDX3X links NLRP11 to the regulation of type I interferon responses and NLRP3 inflammasome activation. *Front. Immunol.* **12**, 653883 (2021).
47. Komatsu, T. et al. Sendai virus V protein inhibits the secretion of interleukin-1 β by preventing NLRP3 inflammasome assembly. *J. Virol.* **92**, e00842–18 (2018).
48. Ratsimandresy, R. A., Dorfleutner, A. & Stehlik, C. An update on PYRIN domain-containing pattern recognition receptors: from immunity to pathology. *Front Immunol.* **4**, 440 (2013).
49. Mangan, M. S. J. et al. Targeting the NLRP3 inflammasome in inflammatory diseases. *Nat. Rev. Drug Discov.* **17**, 588–606 (2018).

Publisher's note Springer Nature remains neutral with regard to jurisdictional claims in published maps and institutional affiliations.



Open Access This article is licensed under a Creative Commons Attribution 4.0 International License, which permits use, sharing, adaptation, distribution and reproduction in any medium or format, as long as you give appropriate credit to the original author(s) and the source, provide a link to the Creative Commons license, and indicate if changes were made. The images or other third party material in this article are included in the article's Creative Commons license, unless indicated otherwise in a credit line to the material. If material is not included in the article's Creative Commons license and your intended use is not permitted by statutory regulation or exceeds the permitted use, you will need to obtain permission directly from the copyright holder. To view a copy of this license, visit <http://creativecommons.org/licenses/by/4.0/>.

© The Author(s) 2022

Methods

Reagents and antibodies. The following antibodies were used: custom-raised NLRP11 rabbit polyclonal (AAMRTSNTASRQPL) and mouse monoclonal (recombinant, amino acids 105–624 and WSLKEGREIGVTPA), NLRP11 rabbit polyclonal antibodies (ab105408, Abcam; HPA0046402, Millipore-Sigma and NBP1-92186, Novus Biologicals), NLRP3 mouse monoclonal (Cryo-2, Adipogen) and rabbit monoclonal (D4D8T, Cell Signaling Technology), ASC rabbit polyclonal (N-15, Santa Cruz Biotechnology), ASC rabbit polyclonal and mouse monoclonal^{13,50}, caspase-1 rabbit monoclonal (D7F10, Cell Signaling Technology), cleaved caspase-1 rabbit monoclonal (D57A2, Cell Signaling Technology), GSDMD rabbit monoclonal (L60, Cell Signaling Technology), cleaved GSDMD rabbit monoclonal (E7H9G, Cell Signaling Technology), caspase-4 rabbit polyclonal (4450, Cell Signaling Technology), NEK7 rabbit monoclonal (EPR4900, Abcam), TGN46 rabbit monoclonal (JF1-024, Invitrogen, rabbit polyclonal Tom20 (FL-145, Santa Cruz Biotechnology), c-myc mouse monoclonal (9E10, Santa Cruz Biotechnology and 9B11, Cell Signaling Technology), HA mouse monoclonal (F-7, Santa Cruz Biotechnology), mouse monoclonal Flag (M2, Millipore-Sigma), mouse monoclonal tubulin (AA12.1, DSHB), rabbit polyclonal vinculin (AB6039, Millipore-Sigma) antibodies, mouse monoclonal Flag agarose (M2, Millipore-Sigma), mouse monoclonal HA agarose (HA-7, Millipore-Sigma) and HRP-conjugated anti-mouse, anti-rabbit and anti-goat IgG (H + L) (Invitrogen), and goat anti-rabbit and anti-mouse Alexa Fluor 488-, 546- and 647-conjugated antibodies (Invitrogen). Antibodies were also used as directly HRP-conjugates for western blot detection of coimmunoprecipitation experiments.

Cell culture. THP-1 cells (TIB-202, ATCC) were maintained in RPMI 1640 media, supplemented with 10% FBS, 1 mM HEPES buffer, 2 mM glutamine, 1 mM sodium pyruvate, 100 IU ml⁻¹ penicillin, 1 mg ml⁻¹ streptomycin and 0.05 mM 2-mercaptoethanol; used at low passage numbers; and screened routinely for mycoplasma infections (MycAlert, Lonza). Blood from healthy donors was drawn by the Cedars Sinai Blood Bank after obtaining informed consent under a protocol approved by Cedars Sinai Institutional Review Board and deidentified. Human peripheral blood mononuclear cells were isolated by Ficoll-Hypaque centrifugation (Millipore-Sigma) from healthy donor buffy coats and countercentrifugal elutriation in the presence of 10 µg ml⁻¹ polymyxin B using a JE-6B rotor (Beckman Coulter), as described earlier⁵¹. To ensure the purity of peripheral blood mononuclear cells, cells were washed in Hank's buffered salt solution and resuspended in serum-free RPMI for 1 h, followed by culturing in complete medium supplemented with 20% FBS for 7 days to differentiate peripheral blood macrophages, which were then cultured in medium supplemented with 10% FBS. Isolated and differentiated peripheral blood macrophages were routinely phenotyped to ensure >85% purity, as determined by flow cytometry for CD45 and CD14. HEK293 cells (CRL-3216, ATCC) and Lenti-X HEK293 cells (632180, Takara Bio) were maintained in DMEM containing 10% FBS, 100 IU ml⁻¹ penicillin and 1 mg ml⁻¹ streptomycin. THP-1 cells or primary human macrophages were primed with ultrapure LPS (0111:B4, 200 ng ml⁻¹, Invivogen, 4h) or Pam3CSK4 (1 µg ml⁻¹, Invivogen, 4h). Where indicated, cells were also treated with nigericin (5 µM, Invivogen, 10–45 min), CTB (20 µg ml⁻¹, List Biological Laboratories, 6h), silica (200 µg ml⁻¹, Invivogen, 6h), TcdB (10 µg ml⁻¹, R&D Systems, 8h) and ATP (5 mM, Millipore-Sigma, 25 min); cultured in K⁺-free medium (0.8 mM MgCl₂, 1.5 mM CaCl₂, 10 mM HEPES, 5 mM glucose and 140 mM NaCl, pH 7.2, 3h)⁵⁰; or transfected with flagellin (500 ng ml⁻¹, Invivogen, 4h), poly(dA:dT) (1 µg ml⁻¹, Invivogen, 4h) or FSL-1 (0.2 µg ml⁻¹, Invivogen, 4h) and ultrapure LPS (1 µg ml⁻¹, 4h) with Lipofectamine 2000 (Invitrogen) or as otherwise indicated.

Gene expression, silencing and knockout. NLRP11 cDNA was amplified by PCR from a human cDNA library cloned into custom pcDNA3 or pLEX expression vectors with Myc, Flag or EGFP tags. NLRP11-TAP was cloned into pHIV-IRES-dTomato (a gift from B. Welm, Addgene, plasmid 21374). Myc-tagged NLRP3^{R260W} was generated previously¹³ and subcloned into pCIG3 (pCMV-IRES-GFPv3; a gift from F. Goodrum, Addgene, plasmid 78264)⁵². NLRP11^{ΔPYD} (aa 104–1,033), NLRP11^{ΔNACHT} (Δ aa 104–560), NLRP11^{ΔLRR} (aa 1–560), NLRP11^{PYD} (aa 1–91), NLRP11^{NACHT} (aa 105–624), NLRP11^{LRR} (aa 560–1,033), NLRP3^{PYD} (aa 1–89), NLRP3^{NACHT} (aa 220–389), NOD1^{NACHT} (aa 133–435), NLRP12^{NACHT} (aa 212–528) and NLR4 were synthesized (IDT, Genewiz) or generated by PCR, cloned into modified pcDNA3 and pHIV-IRES-dTomato expression plasmids. pcDNA3-ASC^{PYD} (aa 1–91), NLRP3 and pyrin have been described earlier^{51,53,54}. All expression constructs were sequence verified. To express or restore NLRP11, NLRP11^{ΔPYD}, NLRP11^{ΔNACHT}, NLRP11^{ΔLRR}, NLRP11^{PYD}, NLRP11^{NACHT}, NLRP11^{LRR} or NLRP3^{R260W} in THP-1 cells, recombinant lentivirus was produced in Lenti-X HEK293 cells by Xfect (Takara Bio) or Lipofectamine 2000 (Invitrogen)-based transfection with modified pLEX (Open Biosystems), pHIV-IRES-dTomato or pCIG3 expression plasmids encoding NLRP3^{R260W}, Myc-NLRP11, NLRP11-Flag, NLRP11^{ΔPYD}-Flag, NLRP11^{ΔNACHT}-Flag, NLRP11^{ΔLRR}-Flag, NLRP11^{PYD}-Flag, NLRP11^{NACHT}-Flag or NLRP11^{LRR}-Flag using empty Myc and Flag vector controls and the viral packaging plasmids psPAX2 (a gift from D. Trono, Addgene, plasmid 12259) and psPAX3 (a gift from D. Trono, Addgene, plasmid 12260), followed by 0.45 µm filtration of virus-containing culture SNs. THP-1 cells were transduced with lentiviral particles in the

presence of polybrene (0.45 µg ml⁻¹) and MISSION ExpressMag magnetic beads (Millipore-Sigma). Cells were puromycin selected (1 µg ml⁻¹) 48 h after infection for 2 weeks and sorted by flow cytometry for comparable NLRP3^{R260W}, NLRP11 or truncated NLRP11 expression. NLRP11- and NLRP11^{ΔPYD}-expressing THP-1 cells were further sorted into low- and high-expressing cell populations and expression verified and normalized by immunoblot.

siRNA-mediated silencing of *NLRP11* was achieved by electroporation or transfection of pooled *NLRP11* siRNA#1 (sc-61142, Santa Cruz Biotechnology) and siRNA#2 (caacaaagaauucagaua; Thermo Scientific) and non-targeting control siRNAs (Santa Cruz Biotechnology and Thermo Scientific). The siRNA for *NLRP3* has been described⁵¹. 1.5 × 10⁶ THP-1 cells were electroporated with single or pooled siRNA duplexes (120 nM) using the Neon Transfection System (Invitrogen) (voltage, 1,600 V; width, 10 ms; three pulses). Primary human macrophages were transfected using F2/virofect (Targeting Systems) and analyzed 72 h after transfection, as described earlier^{50,51,55,56}.

shRNA-mediated *NLRP11*^{KD} was achieved via recombinant lentiviral particles produced as described above. Four distinct shRNAs were cloned into pLKO.1 vector (Addgene, plasmid 10878)⁵⁷. shRNA#1: 5'-ccggcaaacctataaagacgctta ctcgagtaacggtcttatgagtggtttttg-3'; shRNA#2: 5'-ccggcaactcagctgttggtgaact caggtattaccacaatcagctgagtggtttttg-3'; shRNA#3: 5'-ccggcgttacaagttacattctcga gaagtgtatgaactgtaacggtttttg-3'; shRNA#4: 5'-ccgggatcgaagagaattaggactcagtag tccttaattcttcgactttttg-3' (Sigma: TRCN0000128196, TRCN0000149602, TRCN0000146572, TRCN0000128281, respectively). shNLRP11#1 was produced using shRNA#1 and shNLRP11#2 was produced from a virus pool containing all four shRNAs.

NLRP11^{KO} THP-1 cells were generated by CRISPR/Cas9 targeting. Four gRNAs were designed with E-CRISP and CHOPCHOP: gRNA#1: 5'-gagaagcaagatggcagaat-3'; gRNA#2: 5'-ctgttgccaactctctatg-3'; gRNA#3: 5'-gtgttgccaactctctatg-3'; gRNA#4: 5'-tgctgaaggaagctgttagg-3' using lentiCRISPRv1 (Addgene, plasmid 49535)⁵⁸ and control lentiCRISPRv1 (Cas9^{Ctrl}). Cells were puromycin selected (1 µg ml⁻¹) and individual cells were sequence analyzed following PCR amplification of the targeting sequence (forward: 5'-tgccaagatcagtcgacaag-3'; reverse: 5'-ggaagtgtgagaggaggtg-3'). To eliminate potential expression of any alternative spliced NLRP11, we sequentially targeted the NACHT/NAD by transient electroporation of gRNAs cloned into pSpCas9(BB)-2A-GFP (Addgene, plasmid 48138) or empty vector⁵⁹ with 4–7 µg endotoxin-free plasmid as described above. gRNA#1: 5'-ggagaaaattcagctgcaaa-3'; gRNA#2: 5'-gcagctcgaatggggaaga-3'; gRNA#3: 5'-gctcggcaaaagaatttcg-3'; gRNA#4: 5'-cgatgtagacagcttcaag-3'. Cells were FACS selected and individual cells were sequence analyzed following PCR amplification of the targeting sequence (forward 1: 5'-aatcgttgaactcggagg-3'; reverse 1: 5'-agaaacagctcctctcagc-3'; forward 2: 5'-ccgagtcgcaactctatgct-3'; reverse 2: 5'-aagttctcagtcggcccgag-3'). gRNA#4 resulted in a premature stop within the NACHT/NAD. *CASP4*^{KO} THP-1 cells were generated by CRISPR/Cas9 using lentiCRISPRv1 (Addgene, plasmid 49535)⁵⁸. *CASP4* gRNA: 5'-tggtgtttggataactgg-3' and Ctrl gRNA: 5'-accgaggaactgagctgcaaa-3'. *NLRP3*^{KO}, *CASP1*^{KO}, and *ASC*^{KO} cells were described earlier^{13,25}.

Immunoprecipitation. HEK293 cells were transiently transfected with NACHT or PYD constructs in 12-well plates (Lipofectamine 2000, Invitrogen) and analyzed 36 h post transfection. For coimmunoprecipitation of transiently transfected HEK293 cells, cells were washed and lysed in 50 mM HEPES, pH 7.4, 10% Glycerol, 2 mM EDTA, 1% NP-40, supplemented with protease inhibitors using 100 mM NaCl (PYRIN domain), 150 mM NaCl (LRR), 180–800 mM NaCl (NACHT domain), or lysed in RIPA buffer (10 mM Tris-HCl, pH 8.0, 1 mM EDTA, 0.5 mM EGTA, 1% Triton X-100, 0.1% sodium deoxycholate, 0.1% SDS and 140 mM NaCl) supplemented with protease inhibitors (NACHT domain). THP-1 cells were treated as indicated, washed and lysed in 50 mM HEPES, pH 7.4, 50–150 mM NaCl, 10% glycerol, 2 mM EDTA, 0.5% Triton X-100, supplemented with protease inhibitors. For coimmunoprecipitation of culture SNs, conditioned media were adjusted to 0.1% Triton X-100 and supplemented with protease inhibitors and washed with 50 mM NaCl and 0.1% Triton X-100. For IP of endogenous NLRP11, cells were lysed in RIPA buffer (10 mM Tris-HCl, pH 8.0, 1 mM EDTA, 0.5 mM EGTA, 1% Triton X-100, 0.1% sodium deoxycholate, 0.1% SDS and 140 mM NaCl), supplemented with protease and phosphatase inhibitors. Cleared lysates were subjected to IP by incubating with immobilized antibodies or primary antibodies and agarose A/G beads (Santa Cruz Biotechnology) as indicated for 4–16 h at 4°C. Following extensive washing with lysis buffer, bound proteins in Laemmli sample buffer were separated by SDS/PAGE, transferred to polyvinylidene fluoride membranes, blocked (5% non-fat dry milk, 0.1 M Tris-buffered saline, pH 7.4, 0.1% Tween 20) and analyzed by immunoblotting as indicated using HRP-conjugated primary or secondary antibodies. ECL detection (SuperSignal West Femto, Thermo Scientific), and digital image acquisition (Thermo iBright and Ultrasum Omega 14vR). TCL (5%) were also analyzed where indicated. To re-use membranes, bound antibodies were stripped (0.1 M Glycine, 2% SDS) and washed (0.1 M Tris-buffered saline, pH 7.4, 0.1% Tween 20).

Immunoblot. TCLs were directly collected in Laemmli buffer and serum-free culture SNs were collected, adjusted to 5% (v/v) ice-cold Trichloroacetic acid (TCA), incubated on ice for 10 min and centrifuged at 21,000×g for 5 min. Pellets

were washed twice with ice-cold acetone, briefly air-dried and resuspended in Laemmli buffer, sonicated and analyzed by SDS/PAGE/immunoblot as described above.

Immunofluorescence analysis. THP-1 cells were differentiated using PMA (20 nM, 16 h) on coverslips in 12-well plates (0.5×10^6 cells per well), washed in PBS and rested for 48 h before treatment. HEK293 cells were transiently transfected and then seeded onto coverslips. Cells were fixed (3.7% paraformaldehyde in PBS, 20 min, room temperature), permeabilized (0.5% Triton X-100 in PBS, 10 min, room temperature), blocked (2% BSA, 2% (v/v) goat sera, 0.5% Triton X-100 in PBS, 1 h, room temperature), immunostained overnight with primary antibodies in a humidified chamber, washed and subsequently incubated with Alexa Fluor-conjugated secondary antibodies for 1 h, washed and mounted onto slides with Prolong glass antifade mountant with NucBlue stain (Invitrogen). Images were captured on a Nikon TE2000E2-PFS with $\times 60$ and $\times 100$ oil objectives) with image deconvolution (NIS Elements) and a Zeiss LSM 780.

qPCR. Total RNA was isolated from cells using the E.Z.N.A. total RNA isolation Kit (Omega Bio-tek), incubated with DNase I and reverse transcribed (Verso cDNA Synthesis Kit, Thermo Scientific). Multiplexed gene expression analysis was performed on an ABI 7300 Real-Time PCR Machine (Applied Biosystems) and Quantstudio 3 (Thermo Scientific) and displayed as relative expression compared to *ACTB*, using FAM-labeled exon-spanning primers for *IL1B* (Hs01555410_m1), *NLRP11* (Hs00935472_m1), and *NLRP3* (Hs00918082_m1) in combination with VIC-labeled primers for *ACTB* (Hs99999903_m1) (Invitrogen).

ELISA. Cells were seeded into six-well plates (10^6 cells per well) and treated as indicated, and cleared culture SNs were analyzed for IL-1 β (Invitrogen), IL-18 (R&D Systems), IL-6 (BD Biosciences) or TNF (Invitrogen) secretion by ELISA according to the manufacturer's instructions.

LDH cytotoxicity assay. LDH activity was determined using the LDH Cytotoxicity Detection Kit (Takara Bio) in freshly collected culture SNs. Cytotoxicity was defined as a percentage of released LDH compared to total LDH activity upon cell lysis with 1% Triton X-100.

Caspase-1 activity by FLICA. Primed THP-1 cells were treated with nigericin (5 μ M, Invivogen, 45 min) or transfected with poly(dA:dT) (6 ng ml $^{-1}$, Invivogen, 4 h) and simultaneously incubated with a cell-permeable, biotin labeled irreversible caspase-1 inhibitor substrate (YVAD-CMK, 20 μ M) (AnaSpec). Cells were washed twice with cold PBS, fixed with 2% paraformaldehyde (Electron Microscopy Sciences) for 20 min, washed twice with PBS, permeabilized with Cytotfix/Cytoperm (BD Biosciences) for 20 min at 4°C, washed twice with Perm/Wash buffer (BD Biosciences), stained with Alexa Fluor 647-conjugated Streptavidin (Invitrogen) and washed twice with Perm/Wash buffer. Cells were then washed twice with cold autoMACS Running Buffer (Miltenyi Biotec), resuspended in autoMACS Running Buffer and analyzed on an LSR II (BD Biosciences) and Northern Lights (Cytex) instruments. Data were analyzed with FlowJo v10 software (TreeStar).

ASC polymerization assay (crosslinking of TCLs). Cells were rinsed with ice-cold PBS and lysed in 20 mM HEPES, pH 7.4, 100 mM NaCl, 1% NP-40, 1 mM sodium orthovanadate, supplemented with protease inhibitors, followed by shearing with a 27-gauge needle. Insoluble pellets were resuspended in PBS supplemented with 2 mM disuccinimidyl suberate (Pierce) and incubated under rotation at room temperature for 30 min. Samples were centrifuged at 2,348 \times g for 10 min at 4°C, and crosslinked pellets and cleared cell lysates were resuspended in Laemmli sample buffer and analyzed by immunoblot for ASC.

ASC polymerization and NLRP3 oligomerization by immunofluorescence. HEK293 cells were stably transfected with ASC-EGFP or transiently transfected for NLRP3-EGFP and low-expressing clones were selected by limited dilution to prevent spontaneous aggregation and were grown on poly-lysine-coated coverslips. THP-1 cells were differentiated using PMA (20 nM, 16 h) on coverslips, washed in PBS and rested for 48 h before treatment and stained with mouse monoclonal anti-NLRP3 and secondary anti-mouse Alexa Fluor 488-conjugated antibodies. Cells were processed as described above and ASC and NLRP3 oligomerization was quantified using Fiji and normalized to cell numbers⁵⁰.

NLRP3 oligomerization by blue native polyacrylamide gel electrophoresis. For blue native polyacrylamide gel electrophoresis (Invitrogen), cells were lysed in 50 mM Bis-Tris, pH 7.2, 50 mM NaCl, 10% glycerol, 0.0001% Ponceau, 1% digitonin, 2 mM Na₂VO₄, 1 mM sodium fluoride and 1 mM PMSE, supplemented with 1 \times Protease Inhibitor Cocktail (Roche) for 30 min on ice. TCLs were triturated ten times per sample and clarified by centrifugation (16,000 \times g) for 30 min at 4°C and analyzed on blue native polyacrylamide gels (Invitrogen), transferred onto polyvinylidene fluoride membranes and analyzed for NLRP3 or NLRP11 (Flag) expression by immunoblot.

PLA. PLA (Duolink PLA, Millipore-Sigma) was performed according to the manufacturer's instructions. Briefly, THP-1 cells were differentiated using PMA (20 nM, 16 h) on coverslips, washed in PBS and rested for 48 h. Following treatment, cells were washed with PBS, fixed with 3.7% paraformaldehyde for 10 min at room temperature, permeabilized with 0.2% Triton X-100 for 10 min at room temperature and washed with PBS. All incubations were performed in a humidified chamber at 37°C. Cells were blocked with Duolink Blocking Solution for 1 h, followed by incubation with primary antibodies in Duolink Antibody Diluent for 2 h, incubated with PLUS and MINUS PLA probes, washed (Buffer A) at room temperature, incubated with Ligase for 30 min, washed (Buffer A), incubated with polymerase for 100 min, washed (Buffer B) and mounted on slides using a Duolink In Situ Mounting Medium with DAPI. Cells were analyzed by confocal microscopy (Zeiss, LSM 780).

Statistics and reproducibility. All representative results were independently repeated at least three times with similar results, and *n* indicates the number of biological replicates. Graphs were prepared in Prism 9 (GraphPad) and data are presented as mean values \pm s.d. A standard two-tailed unpaired *t*-test was used for pairwise statistical analysis of all data. Values of *P* < 0.05 were considered significant (and marked by an asterisk), and *P* values are listed in the figure legends.

Reporting Summary. Further information on research design is available in the Nature Research Reporting Summary linked to this article.

Data availability

All data sets are provided as source data, and additional information is available from the corresponding authors upon reasonable request. Source data of intact immunoblots are included for Fig. 1, Fig. 2, Fig. 3, Fig. 4, Fig. 5, Fig. 6, Fig. 7, Extended Data Fig. 1, Extended Data Fig. 2, Extended Data Fig. 5, Extended Data Fig. 6 and Extended Data Fig. 7. Source data of graphs are included for Fig. 1, Fig. 2, Fig. 4, Fig. 5, Fig. 6, Fig. 7, Extended Data Fig. 1 and Extended Data Fig. 3. Source data are provided with this paper.

References

- de Almeida, L. et al. The PYRIN domain-only protein POP1 inhibits inflammasome assembly and ameliorates inflammatory disease. *Immunity* **43**, 264–276 (2015).
- Khare, S. et al. An NLRP7-containing inflammasome mediates recognition of microbial lipopeptides in human macrophages. *Immunity* **36**, 464–476 (2012).
- Caviness, K., Cicchini, L., Rak, M., Umashankar, M. & Goodrum, F. Complex expression of the UL136 gene of human cytomegalovirus results in multiple protein isoforms with unique roles in replication. *J. Virol.* **88**, 14412–14425 (2014).
- Stehlik, C. et al. Apoptosis-associated speck-like protein containing a caspase recruitment domain is a regulator of procaspase-1 activation. *J. Immunol.* **171**, 6154–6163 (2003).
- Stehlik, C. et al. The PAAD/PYRIN-only protein POP1/ASC2 is a modulator of ASC-mediated NF- κ B and pro-caspase-1 regulation. *Biochem J.* **373**, 101–113 (2003).
- Khare, S. et al. The PYRIN domain-only protein POP3 inhibits ALR inflammasomes and regulates responses to infection with DNA viruses. *Nat. Immunol.* **15**, 343–353 (2014).
- Ratsimandresy, R. A. et al. The PYRIN domain-only protein POP2 inhibits inflammasome priming and activation. *Nat. Commun.* **8**, 15556 (2017).
- Moffat, J. et al. A lentiviral RNAi library for human and mouse genes applied to an arrayed viral high-content screen. *Cell* **124**, 1283–1298 (2006).
- Shalem, O. et al. Genome-scale CRISPR-Cas9 knockout screening in human cells. *Science* **343**, 84–87 (2014).
- Ran, F. A. et al. Genome engineering using the CRISPR-Cas9 system. *Nat. Protoc.* **8**, 2281–2308 (2013).
- Schindelin, J. et al. Fiji: an open-source platform for biological-image analysis. *Nat. Methods* **9**, 676–682 (2012).

Acknowledgements

psPAX2 and pMD.2G were a gift from D. Trono, pSpCas9(BB)-2A-GFP and lentiCRISPRv1 were a gift from F. Zhang, pHIV-IRES-dTomato was a gift from B. Welm and pCMV-IRES-GFPv3 was a gift from F. Goodrum. This work was supported by the National Institutes of Health (grants AI099009 and AR064349 to C.S. and grants AI134030, AI140702, AI165797 and AI120625 to C.S. and A.D.) and the American Heart Association (grant 834502 to J.C.).

Author contributions

All authors contributed to the design of experiments, performed experiments, analyzed results, prepared preliminary figures and provided critical review of the manuscript. A.D. and C.S. conceived the study, provided overall direction, designed the research and performed the initial experiments, prepared the final figures and wrote the manuscript. A.G. generated the *NLRP11*^{KO} and *NLRP11*^{KO} cells; initially introduced NLRP11 in *NLRP11*^{KO} and *NLRP3*^{KO} cells; generated the *NLRP3*^{R26W} and *NLRP11*^{Myc}

cells; quantified initial ASC and NLRP3 aggregates in HEK293 cells; contributed to the FLICA assay; performed some of the microscopy of NLRP11 in HEK293 and THP-1 cells; performed the preliminary PYD coimmunoprecipitation experiments and ASC crosslinking in *NLRP11*^{KO} and transiently transfected HEK293 cells; contributed to some of the native gels; contributed to the PLA; performed cytokine analysis in *NLRP11*^{KO} cells, *NLRP11*^{siRNA} transfected cells, NLRP11-expressing *NLRP3*^{KO}/*NLRP11*^{Flag} cells, *NLRP11*^{KO}/*NLRP3*^{R260W} cells and some of the NLRP11(lo) and NLRP11(hi) restored cells and in *NLRP11*^{Myc} cells; and performed the LDH assays and endogenous interaction of NLRP3 and NLRP11. These contributions are reflected as the only contributor to Figs. 1a,b,d,h,k, 2g,h, 3a,b,d, 4a,e-g, 5a,b, 6b,e,k and 7a-d,f, Extended Data Fig. 1a,b, Extended Data Fig. 3 and Extended Data Fig. 5c and shared contributor to Fig. 1j (panel 1), Fig. 2a-d, Fig. 5f,g and Fig. 6a,j. S.D. performed most of the cytokine analysis in *NLRP11*^{KO}, *CASP4*^{KO}, *CASP1*^{KO} and *NLRP3*^{KO} cells; performed the caspase-1 and GSDMD cleavage analysis, inflammasome complex purification assays in *NLRP11*^{KO}, *NLRP11*^{Flag}, *NLRP11*^{ΔPYD-Flag}, *NLRP3*^{KO}, *ASC*^{KD}, *NLRP3*^{KO}/*NLRP11*^{Flag}, *ASC*^{KD}/*NLRP11*^{Flag} THP-1 cells, the interaction analysis of NLRP3 and NEK7 and ASC crosslinking in *NLRP11*^{Flag} and *NLRP11*^{ΔPYD-Flag} cells; and contributed or performed the blue native gels, the cytokine analysis in *NLRP11*^{ΔPYD-Flag} cells. These contributions are reflected as the only contributor to Figs. 1e, 1f,g, 2e, 3c,e, 4c,d,h, 5h and 6d,i, Extended Data Fig. 2g and Extended Data Fig. 7c and shared contributor to (Figs. 1j (panels 2 and 3) and 5f,g). S.T. generated the THP-1 cell lines restored with varying *NLRP11*^{Flag} and *NLRP11*^{ΔPYD-Flag} expression all the *NLRP11* single domain and single domain deletion restored cells, the *NLRP3*^{KO}/*NLRP11*^{Flag} and *ASC*^{KD}/*NLRP11*^{Flag} cells, regenerated the *NLRP3*^{R260W} cells, sorted cells for comparable expression, performed the expression verification of all THP-1 cell lines except *NLRP11*^{Myc} cells and *CASP4*^{KO} cells, performed the *NLRP3*^{EGFP} oligomerization analysis with all *NLRP11* domains in HEK293 cells and THP-1 cells, performed the *NLRP3*^{R260W} oligomerization in THP-1 cells, performed the cytokine analysis in *NLRP11* domain-expressing cells, performed the *NLRP11* complex analysis in the culture SN and performed the microscopy for mitochondria and TGN. These contributions are reflected as the only contributor to Figs. 1c, 5c-e,i, 6c, 7e, Extended Data Fig. 2f, Extended Data

Fig. 5a,b, Extended Data Fig. 6a,b and Extended Data Fig. 8a,b. J.C. performed most of the binding studies in HEK293 cells with PYD and NACHT domains, determined specificity and performed all the LRR binding assays. These contributions are reflected as the only contributor to Figs. 4b, 6f,g,h and Extended Data Fig. 7a,b. H.N. performed some of the cloning and supported the generation of lentiviruses and stable cells. E.J. contributed to the caspase-1 activation assays. These contributions are reflected as the only contributor to Fig. 2f. H.K. performed the qPCR analysis. These contributions are reflected as the only contributor to Fig. 1i and Extended Data Fig. 1c. L.H.C. established and characterized the *CASP1*^{KO} and *CASP4*^{KO} cells, supported the generation of *NLRP11*^{KO} cells and contributed to the PLAs. These contributions are reflected as shared contributor to Fig. 6a,j. R.A.R. contributed to the FLICA experiments. These contributions are reflected as shared contributor to Fig. 2a-d.

Competing interests

The authors declare no competing interests.

Additional information

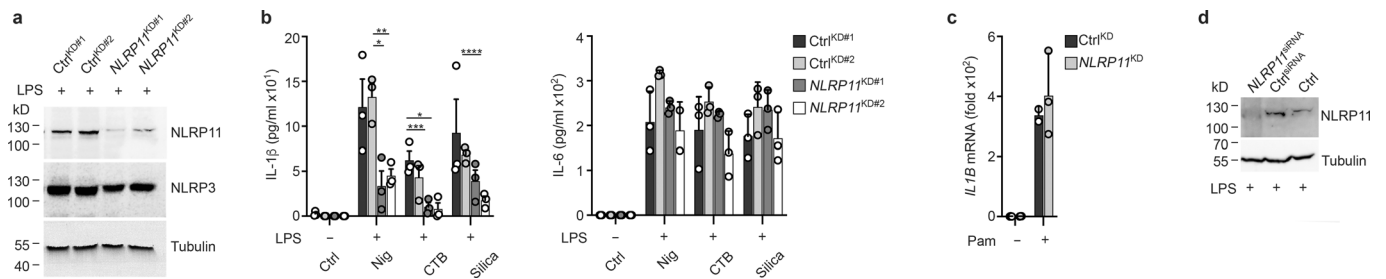
Extended data Extended data are available for this paper at <https://doi.org/10.1038/s41590-022-01220-3>.

Supplementary information The online version contains supplementary material available at <https://doi.org/10.1038/s41590-022-01220-3>.

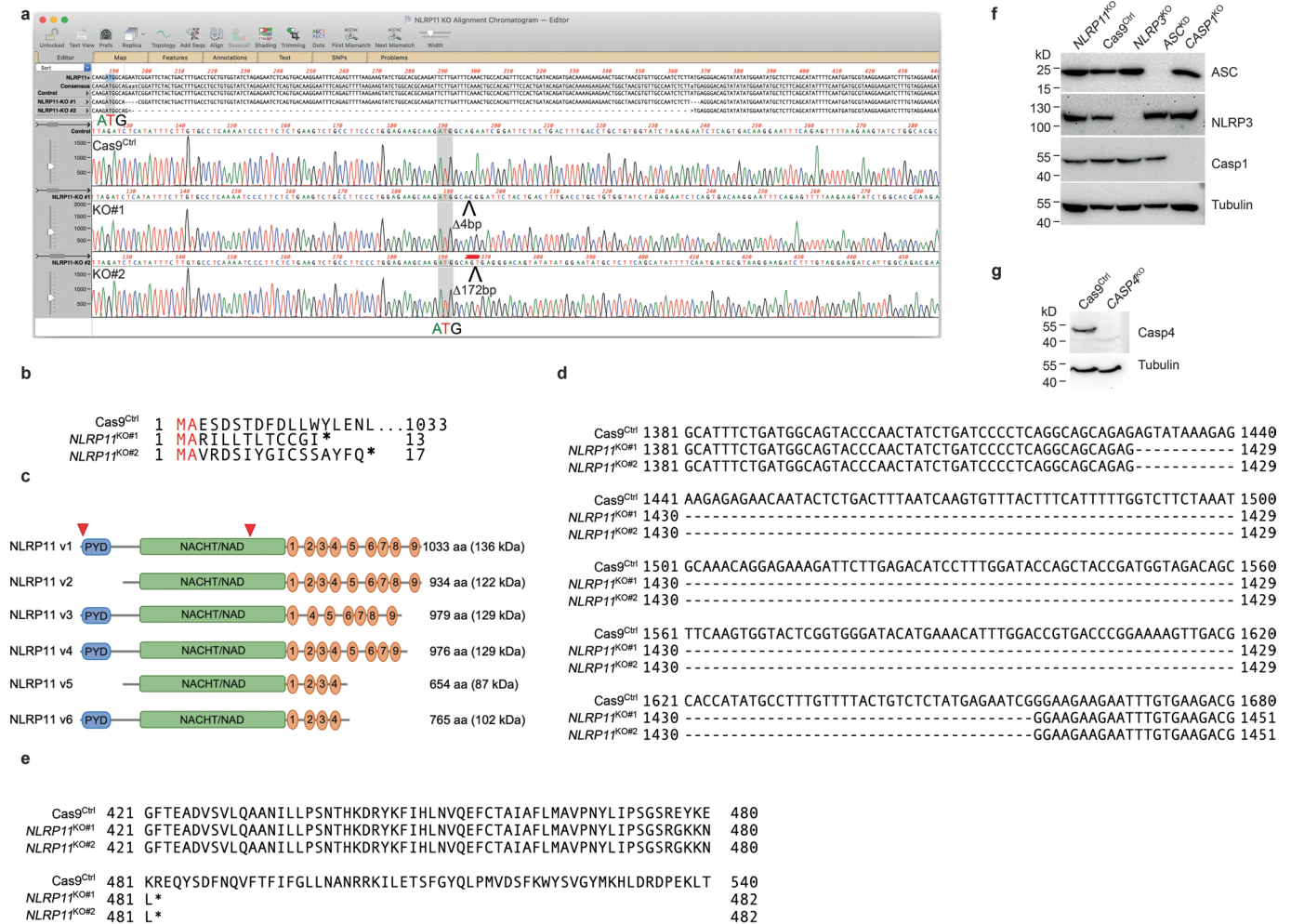
Correspondence and requests for materials should be addressed to Andrea Dorfleutner or Christian Stehlik.

Peer review information *Nature Immunology* thanks Seth Masters and the other, anonymous, reviewer(s) for their contribution to the peer review of this work. Ioana Visan was the primary editor on this article and managed its editorial process and peer review in collaboration with the rest of the editorial team.

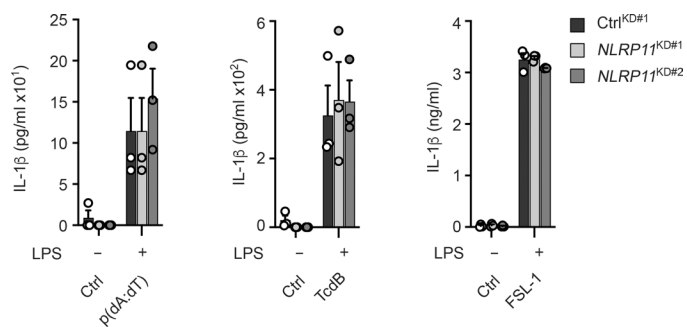
Reprints and permissions information is available at www.nature.com/reprints.



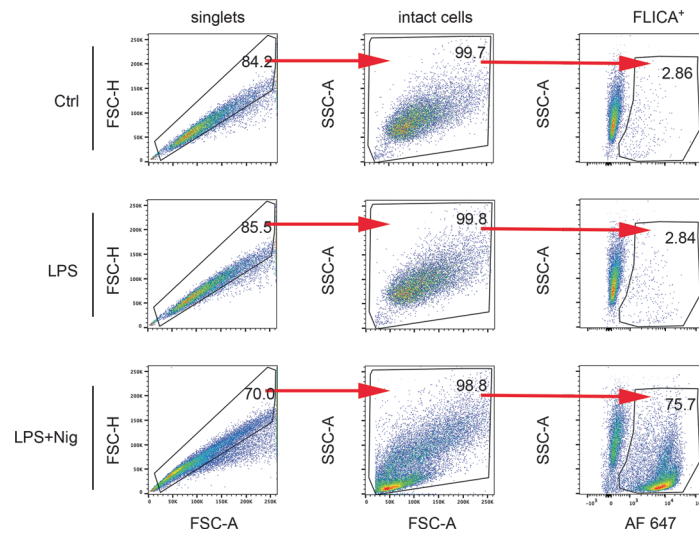
Extended Data Fig. 1 | Knockdown of *NLRP11* impairs NLRP3-mediated cytokine release. (a) Immunoblot for NLRP11, NLRP3 and tubulin loading control using TCL of LPS-primed (200 ng/ml, 4 h) stable control (Ctrl^{KD#1} and Ctrl^{KD#2}) and *NLRP11* knockdown (KD) THP-1 cells (NLRP11^{KD#1} and NLRP11^{KD#2}). **(b)** IL-1 β and IL-6 ELISA of SN from Ctrl^{KD#1}, Ctrl^{KD#2}, NLRP11^{KD#1} and NLRP11^{KD#2} cells left untreated or primed with LPS (200 ng ml⁻¹, 4 h) and primed+activated with Nig (5 μ M, 30 min), CTB (20 μ g ml⁻¹, 6 h) and Silica (200 μ g ml⁻¹, 6 h); (n=3, mean \pm s.d.); *p=0.0121; **p=0.0068, ***p=0.0101, ****p=0.0018. **(c)** Quantitative real-time PCR of *IL1B* mRNA levels from Ctrl^{KD} and NLRP11^{KD} cells left untreated and primed with Pam3CSK4 (1 μ g ml⁻¹, 2 h) and presented as fold induction compared to Ctrl cells (n=3, mean \pm s.d.). **(d)** Immunoblot for NLRP11 and tubulin loading control using TCL of primary human macrophages either not transfected (Ctrl), transfected with Ctrl^{siRNA} or NLRP11^{siRNA} and primed with LPS (200 ng/ml, 4 h).



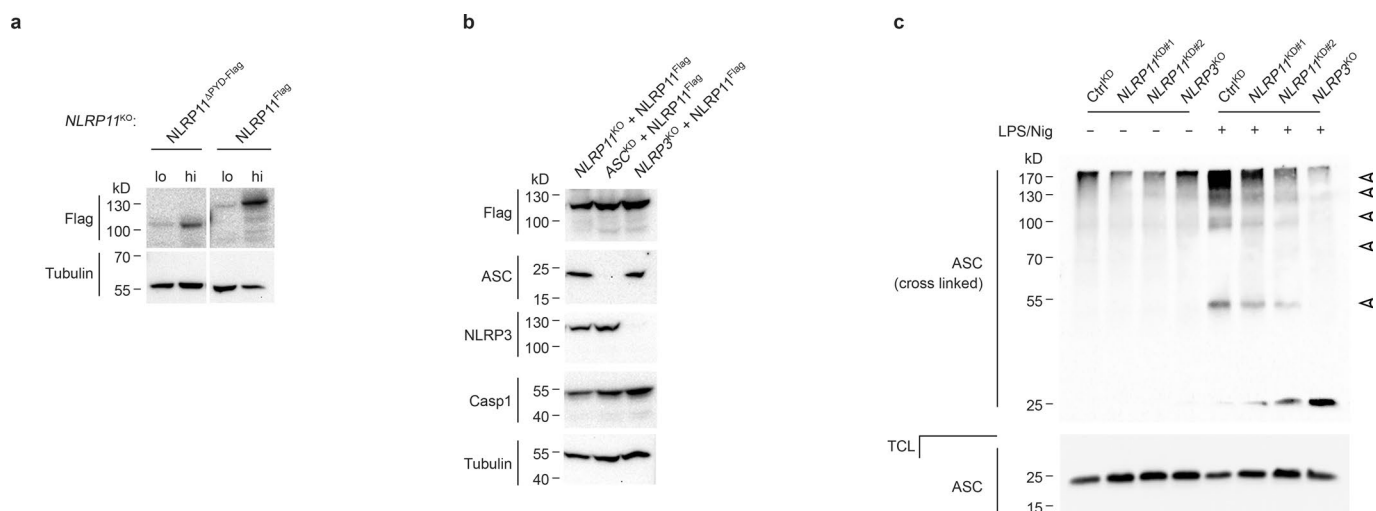
Extended Data Fig. 2 | NLRP11 knockout THP-1 cells. (a) PCR amplification and sequencing analysis of Cas9^{Ctrl}, NLRP1^{KO#1} and NLRP1^{KO#2} THP-1 cells, showing two distinct deletions of 4 and 172 bp. **(b)** The predicted amino acid sequence and protein length of the resulting NLRP11 proteins are indicated, with the premature stop marked by an asterisk. **(c)** Domain architecture of the six predicted NLRP11 isoforms. A red arrowhead marks the 2 gRNA targeting sites. **(d)** PCR amplification and sequence analysis of Cas9^{Ctrl}, NLRP1^{KO#1} and NLRP1^{KO#2} cells showing the 229 bp deletion in the NACHT/NAD. **(e)** The predicted amino acid sequence and protein length of the resulting NLRP11 proteins are indicated, with the premature stop marked by an asterisk. **(f,g)** Immunoblot for **(f)** ASC, NLRP3, Caspase-1 and tubulin loading control using TCL from Cas9^{Ctrl}, NLRP1^{KO#1}, NLRP3^{KO}, ASC^{KO} and CASP1^{KO} cells and **(g)** caspase-4 and tubulin loading control from TCL of Cas9^{Ctrl} and CASP4^{KO} cells.



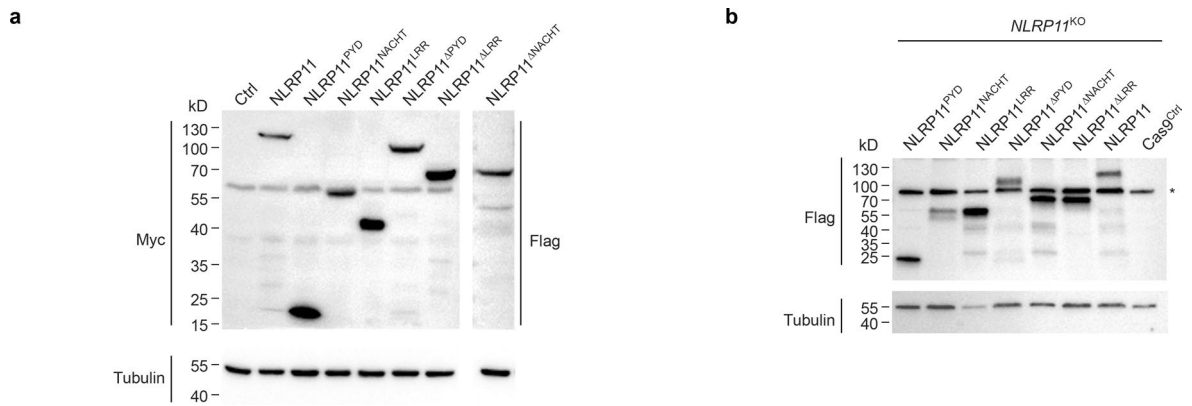
Extended Data Fig. 3 | Knockdown of *NLRP11* does not impair IL-1 β release by non-NLRP3 inflammasomes. IL-1 β ELISA of SN from Ctrl^{KD} and NLRP11^{KD} cells left untreated or primed with LPS (200 ng ml⁻¹, 4 h) and primed+activated with TcdB (10 μ g ml⁻¹, 8 h), transfected with poly(dA:dT) (1 μ g ml⁻¹, 4 h) or FSL-1 (0.2 μ g ml⁻¹, 4 h); (n = 3, mean \pm s.d.).



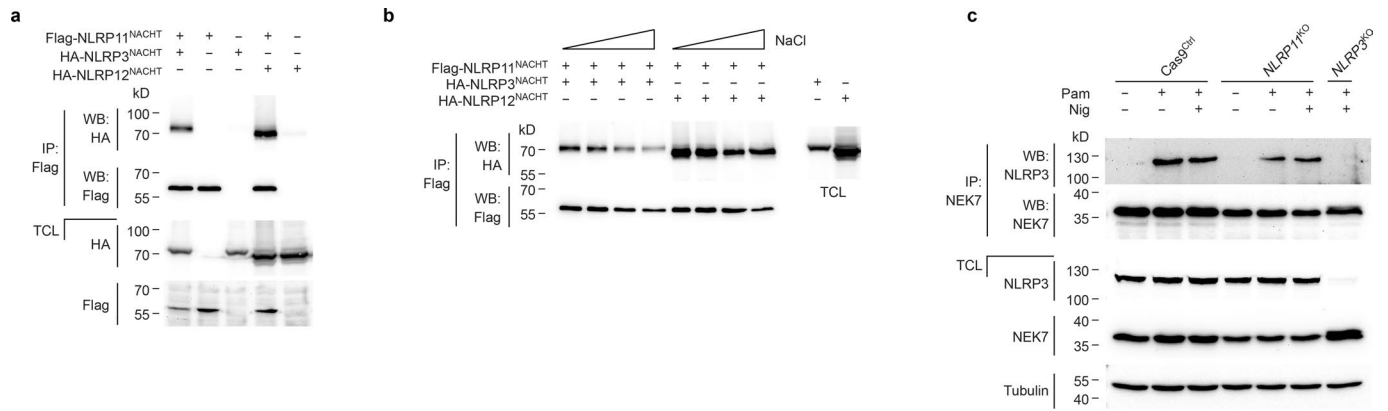
Extended Data Fig. 4 | FLICA gating strategy. Gating strategy used for the FLICA in Fig. 2a-d of Ctrl^{KD#1} cells left untreated, primed with LPS (1 $\mu\text{g ml}^{-1}$, 1h) and primed+activated with Nig (5 μM , 45 min). Total cells were gated for singlets, intact cells and for Alexa Fluor (AF) 647⁺ cells. All samples were gated following this strategy.



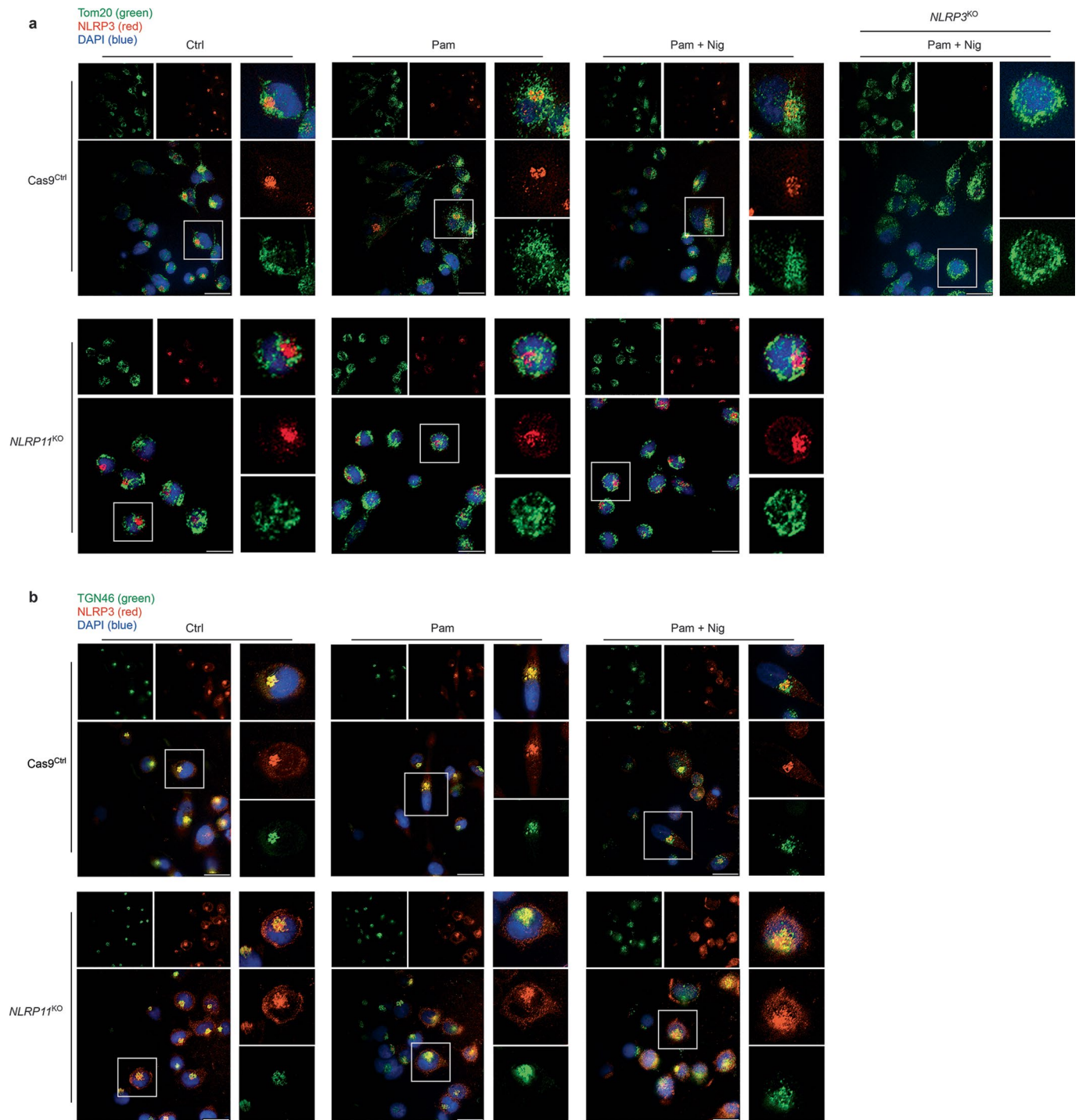
Extended Data Fig. 5 | NLRP11 silencing impairs ASC polymerization. (a) Immunoblot for Flag and tubulin loading control using TCL from NLRP11^{Flag} and NLRP11^{ΔPYD-Flag} cells sorted into low (lo) and high (hi) expressing populations. The gap in the blot indicates removal of additional NLRP11-expressing cell populations not included in this study. **(b)** Immunoblot for Flag, ASC, NLRP3, caspase-1 and tubulin loading control using TCL from NLRP11^{KO}, ASC^{KO} and NLRP3^{KO} cells restored with NLRP11-Flag. **(c)** ASC crosslinking and immunoblot for ASC using TCL and crosslinked TCL from Ctrl^{KO}, NLRP11^{KD#1}, NLRP11^{KD#2}, and NLRP3^{KO} cells left untreated, primed with LPS (200 ng ml⁻¹, 4 h) or primed+activated with Nig (5 μM, 20 min). Arrowheads mark crosslinked ASC polymers.



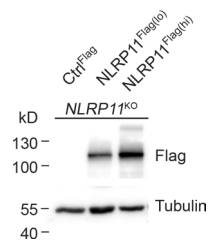
Extended Data Fig. 6 | NLRP11 domain expression for NLRP3 oligomerization. (a) Immunoblot for Myc, Flag and tubulin loading control using TCL from HEK293^{NLRP3-EGFP} cells transiently cotransfected with empty vector (Ctrl), Myc or Flag-tagged NLRP11 or NLRP11 domains as indicated. **(b)** Immunoblot for Flag and tubulin loading control using TCL from *NLRP11*^{KO} THP-1 stably restored with NLRP11-Flag or truncated NLRP11-Flag, as indicated. *marks a cross-reactive protein.



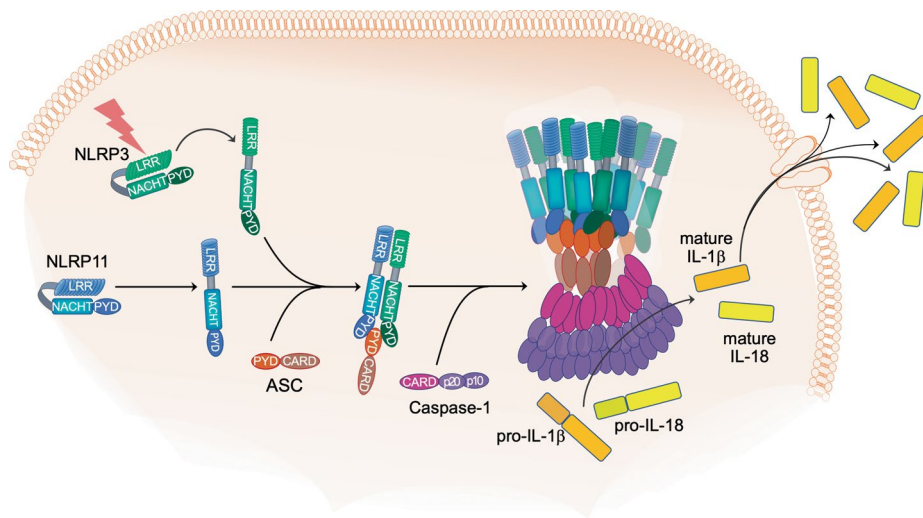
Extended Data Fig. 7 | NLRP11 NACHT interactions and NLRP11 does not affect NEK7 recruitment to NLRP3. (a,b) Immunoprecipitation with immobilized anti-Flag antibodies using TCL from HEK293 cells transiently transfected with Flag-NLRP11^{NACHT}, HA-NLRP3^{NACHT} and HA-NLRP12^{NACHT}, as indicated **(a)** using RIPA buffer and **(b)** washed with increasing NaCl concentrations (200 mM, 400 mM, 600 mM and 800 mM) and immunoblot of IP and TCL for HA and Flag. **(c)** IP with immobilized anti-NEK7 antibodies using TCL from untreated, Pam3CSK4 primed (1 $\mu\text{g ml}^{-1}$, 2 h) and primed+Nig (5 μM , 10 min) activated Cas9^{ctrl}, NLRP11^{KO} and NLRP3^{KO} cells and immunoblot of IP and TCL for NLRP3, NEK7 and tubulin loading control.



Extended Data Fig. 8 | NLRP11 does not affect TGN localization of NLRP3. (a,b) Confocal microscopy of PMA-differentiated Cas9^{Ctrl}, *NLRP11*^{KO} and *NLRP3*^{KO} cells left untreated, primed with Pam3CSK4 (1 $\mu\text{g ml}^{-1}$, 2 h) or primed+activated with Nig (5 μM , 20 min) immunostained for **(a)** Tom20 (green), NLRP3 (red) and DAPI (blue), and **(b)** TGN46 (green), NLRP3 (red) and DAPI (blue).



Extended Data Fig. 9 | Low and high-expressing NLRP11^{Flag} cells. Immunoblot for Flag and tubulin loading control using TCL of Ctrl^{Flag}, NLRP11^{Flag(lo)} and NLRP11^{Flag(hi)} cells.



Extended Data Fig. 10 | An updated model for NLRP3 inflammasome assembly and activation. Human NLRP11 binds ASC by PYRIN domain (PYD)-PYD interaction and to NLRP3 through its NACHT-LRR region, thereby acting as a scaffold for bridging ASC and NLRP3, which facilitates efficient oligomerization of NLRP3 and consequently, enables caspase-1 activation, IL-1 β and IL-18 release and pyroptosis by promoting the polymerization of ASC.

Reporting Summary

Nature Research wishes to improve the reproducibility of the work that we publish. This form provides structure for consistency and transparency in reporting. For further information on Nature Research policies, see our [Editorial Policies](#) and the [Editorial Policy Checklist](#).

Statistics

For all statistical analyses, confirm that the following items are present in the figure legend, table legend, main text, or Methods section.

n/a Confirmed

- | | | |
|-------------------------------------|-------------------------------------|--|
| <input type="checkbox"/> | <input checked="" type="checkbox"/> | The exact sample size (n) for each experimental group/condition, given as a discrete number and unit of measurement |
| <input type="checkbox"/> | <input checked="" type="checkbox"/> | A statement on whether measurements were taken from distinct samples or whether the same sample was measured repeatedly |
| <input type="checkbox"/> | <input checked="" type="checkbox"/> | The statistical test(s) used AND whether they are one- or two-sided
<i>Only common tests should be described solely by name; describe more complex techniques in the Methods section.</i> |
| <input checked="" type="checkbox"/> | <input type="checkbox"/> | A description of all covariates tested |
| <input checked="" type="checkbox"/> | <input type="checkbox"/> | A description of any assumptions or corrections, such as tests of normality and adjustment for multiple comparisons |
| <input type="checkbox"/> | <input checked="" type="checkbox"/> | A full description of the statistical parameters including central tendency (e.g. means) or other basic estimates (e.g. regression coefficient) AND variation (e.g. standard deviation) or associated estimates of uncertainty (e.g. confidence intervals) |
| <input type="checkbox"/> | <input checked="" type="checkbox"/> | For null hypothesis testing, the test statistic (e.g. F , t , r) with confidence intervals, effect sizes, degrees of freedom and P value noted
<i>Give P values as exact values whenever suitable.</i> |
| <input checked="" type="checkbox"/> | <input type="checkbox"/> | For Bayesian analysis, information on the choice of priors and Markov chain Monte Carlo settings |
| <input checked="" type="checkbox"/> | <input type="checkbox"/> | For hierarchical and complex designs, identification of the appropriate level for tests and full reporting of outcomes |
| <input checked="" type="checkbox"/> | <input type="checkbox"/> | Estimates of effect sizes (e.g. Cohen's d , Pearson's r), indicating how they were calculated |

Our web collection on [statistics for biologists](#) contains articles on many of the points above.

Software and code

Policy information about [availability of computer code](#)

Data collection: Nikon NIS Elements Advanced Research 5.2, BD FACSDiva, SKanIT 6.0.2, iBright FL1500 software version 1.7.0, Applied Biosystems QuantStudio3 1.3.3

Data analysis: Adobe Photoshop 2022, Adobe Illustrator 2022, FlowJo 10, Prism Graphpad 9

For manuscripts utilizing custom algorithms or software that are central to the research but not yet described in published literature, software must be made available to editors and reviewers. We strongly encourage code deposition in a community repository (e.g. GitHub). See the Nature Research [guidelines for submitting code & software](#) for further information.

Data

Policy information about [availability of data](#)

All manuscripts must include a [data availability statement](#). This statement should provide the following information, where applicable:

- Accession codes, unique identifiers, or web links for publicly available datasets
- A list of figures that have associated raw data
- A description of any restrictions on data availability

Data are provided as source data and no additional data sets were collected

Field-specific reporting

Please select the one below that is the best fit for your research. If you are not sure, read the appropriate sections before making your selection.

Life sciences Behavioural & social sciences Ecological, evolutionary & environmental sciences

For a reference copy of the document with all sections, see [nature.com/documents/nr-reporting-summary-flat.pdf](https://www.nature.com/documents/nr-reporting-summary-flat.pdf)

Life sciences study design

All studies must disclose on these points even when the disclosure is negative.

Sample size	no pre-determination was performed, internal controls in each experiment with well known effect were used and sample size was based on prior experience
Data exclusions	no data were excluded
Replication	we replicated data at 2 different institutes; asked multiple researchers to replicate key data; used complementary approaches for testing: for example, we used siRNA, shRNA and CRISPR/Cas9 knock out to validate each approach. After pilot optimization, all representative results have been independently repeated at least 3 times with similar results and all "n" refer to biological replicates.
Randomization	no randomization and our study does not involve in vivo experiments. Cell wells were randomly assigned to each treatment group. Samples were collected and analyzed without bias using 2 researchers for sample collection and analysis, when appropriate.
Blinding	no on purpose blinding, but separating sample collection and data collection, when possible and appropriate for ELISA samples.

Reporting for specific materials, systems and methods

We require information from authors about some types of materials, experimental systems and methods used in many studies. Here, indicate whether each material, system or method listed is relevant to your study. If you are not sure if a list item applies to your research, read the appropriate section before selecting a response.

Materials & experimental systems

n/a	Involvement in the study
<input type="checkbox"/>	<input checked="" type="checkbox"/> Antibodies
<input type="checkbox"/>	<input checked="" type="checkbox"/> Eukaryotic cell lines
<input checked="" type="checkbox"/>	<input type="checkbox"/> Palaeontology and archaeology
<input checked="" type="checkbox"/>	<input type="checkbox"/> Animals and other organisms
<input type="checkbox"/>	<input checked="" type="checkbox"/> Human research participants
<input checked="" type="checkbox"/>	<input type="checkbox"/> Clinical data
<input checked="" type="checkbox"/>	<input type="checkbox"/> Dual use research of concern

Methods

n/a	Involvement in the study
<input checked="" type="checkbox"/>	<input type="checkbox"/> ChIP-seq
<input type="checkbox"/>	<input checked="" type="checkbox"/> Flow cytometry
<input checked="" type="checkbox"/>	<input type="checkbox"/> MRI-based neuroimaging

Antibodies

Antibodies used

Rabbit polyclonal anti-NLRP11 (Novus Biologicals, NBP1-92186), (1:1000)
 Rabbit polyclonal anti-NLRP11 (Abcam, ab105408), (1:1000)
 Rabbit polyclonal anti-NLRP11 (Sigma-Aldrich, HPA046402), (1:1000)
 Mouse monoclonal anti-NLRP11 (custom), (1:1000)
 Rabbit polyclonal anti-NLRP11 (custom), (1:1000)
 Rabbit polyclonal anti-ASC (Adipogen, AG-25B-0006-C100, AL177), (1:1000)
 Rabbit polyclonal anti-ASC (custom), (1:1000)
 Mouse monoclonal anti-ASC (custom), (1:1000)
 Mouse monoclonal anti-NLRP3 (Adipogen, Cryo-2), (1:1000)
 Rabbit polyclonal anti-NLRP3 (Cell Signaling Technology, D4D8T), (1:1000)
 Rabbit monoclonal anti-caspase-1 (Cell Signaling Technology, D7F10), (1:1000)
 Rabbit monoclonal anti-cleaved caspase-1 (Cell Signaling Technology, D57A2) (1:1000)
 Rabbit monoclonal anti-GSDMD (Cell Signaling Technology, L60), (1:1000)
 Rabbit monoclonal anti-cleaved GSDMD (Cell Signaling Technology, E7H9G), (1:1000)
 rabbit polyclonal anti-Caspase-4 (Cell Signaling Technology, 4450), (1:1000)
 rabbit monoclonal anti-NEK7 (Abcam, EPR4900), (1:1000)
 rabbit monoclonal anti-TGN46 (Invitrogen, JF1-024), (1:100)
 rabbit polyclonal anti-Tom20 (Santa Cruz Biotechnology, FL-145,), (1:100)
 Mouse monoclonal anti-cMyc (Santa Cruz Biotechnology, 9E10), (1:1000)
 Mouse monoclonal anti-cMyc (Cell Signaling Technology, 9B11), (1:1000)
 Mouse monoclonal anti-HA (Millipore-Sigma, F-7), (1:1000)

Mouse monoclonal anti-FLAG (Millipore-Sigma, M-2), (1:1000)
 Monoclonal anti-FLAG M2-Peroxidase HRP (Sigma, A8592), (1:2000)
 Mouse monoclonal anti-tubulin (DSHB, AA12.1), (1:1000)
 Goat anti-mouse IgG1 HRP (Santa Cruz Biotechnology, sc-2060), (1:10,000)
 Protein A/G PLUS-Agarose (Santa-Cruz Biotechnology, sc-2003), beads
 Anti-HA Magnetic Beads (Thermo Fisher, PI88836), beads
 Anti-DYKDDDDK Magnetic Agarose (Thermo Fisher, A36797), beads
 S-Protein Agarose (EMD Millipore, 69704-3), beads
 Goat anti-Rabbit IgG (H+L) Alexa Fluor 488 (Invitrogen, A32731), (1:100)
 Goat anti-Rabbit IgG (H+L) Alexa Fluor 546 (Invitrogen, A11035), (1:100)
 Goat anti-Rabbit IgG (H+L) Alexa Fluor 647 (Invitrogen, A21245), (1:100)
 Goat anti-Mouse IgG (H+L) Alexa Fluor 488 (Invitrogen, A11029), (1:100)
 Goat anti-Mouse IgG (H+L) Alexa Fluor 546 (Invitrogen, A11030), (1:100)
 Goat anti-Mouse IgG (H+L) Alexa Fluor 647 (Invitrogen, A21235), (1:100)
 PLA probes Rabbit plus (Millipore-Sigma, DUO92002), (1:5)
 PLA probes Mouse Minus (Millipore-Sigma, DUO92004), (1:5)
 In Situ Detection Reagents Green (Millipore-Sigma, DUO92014),
 In Situ Detection Reagents Red (Millipore-Sigma, DUO92008),
 AlexaFluor 647 Streptavidin (Invitrogen, S21374), (1:10000)
 Goat anti-Rabbit IgG (H+L) HRP (Invitrogen, 31460), (1:10000)
 Goat anti-Mouse IgG (H+L) HRP (Invitrogen, A15999), (1:10000)
 VeriBlot for IP Detection Reagent HRP (Abcam, ab131366), (1:200)

Validation

except well established antibodies (tubulin) we tested all antibodies using one of these approaches: epitope tag antibodies: using transient transfection of tagged cDNAs and controls and western blot analysis. Antibodies to inflammasome components were tested in cells with shRNA knock-down or CRISPR/Cas9 knock-out as well as using resting cells and cells with active inflammasome for testing cleaved caspase-1 and GSDMD, release of inflammasome components as well as ELISA assays.

Eukaryotic cell lines

Policy information about [cell lines](#)

Cell line source(s)

HEK293T (ATCC, CRL-3216),
 Lenti-X HEK293 (Takara Bio, 632180),
 THP-1 (ATCC, TIB-202),

Authentication

cell lines were directly obtained from the vendor or ATCC and those with a known genotype (stable expressing cells, knock out cells), were routinely tested by western blot for validation.

Mycoplasma contamination

we routinely test cell lines for Mycoplasma contamination, a statement is included in the methods section. Cells used for experiments tested negative for Mycoplasma.

Commonly misidentified lines (See [ICLAC](#) register)

cell lines used in this study are not commonly misidentified and are not included in this database.

Human research participants

Policy information about [studies involving human research participants](#)

Population characteristics

unknown

Recruitment

as part of blood donation at the Cedars-Sinai Blood Bank or buffy coats purchased from the Red cross

Ethics oversight

The Cedars Sinai Blood Bank obtained informed consent under a protocol approved by Cedars Sinai Institutional Review Board. All samples were de-identified for research staff

Note that full information on the approval of the study protocol must also be provided in the manuscript.

Flow Cytometry

Plots

Confirm that:

- The axis labels state the marker and fluorochrome used (e.g. CD4-FITC).
- The axis scales are clearly visible. Include numbers along axes only for bottom left plot of group (a 'group' is an analysis of identical markers).
- All plots are contour plots with outliers or pseudocolor plots.
- A numerical value for number of cells or percentage (with statistics) is provided.

Methodology

Sample preparation	THP-1 cells were incubated with a cell-permeable, biotin labeled irreversible caspase-1 inhibitor substrate (YVAD-CMK, 20 uM) (AnaSpec). Cells were washed twice with cold PBS, fixed with 2% paraformaldehyde (Electron Microscopy Sciences) for 20m, washed twice with PBS, permeabilized with Cytofix/Cytoperm (BD Biosciences) for 20m at 4°C, washed twice with Perm/Wash buffer (BD Biosciences), stained with Alexa Fluor 647-conjugated Streptavidin (Invitrogen), and washed twice with Perm/Wash buffer. Cells were then washed twice with cold autoMACS Running Buffer (Miltenyi Biotec), resuspended in autoMACS Running Buffer and analyzed
Instrument	BD LSRII
Software	BD FACSDiva
Cell population abundance	this was a simple 1 color analysis and 100% of singlets were included
Gating strategy	FSC-H vs. FSC-A density plot gating was performed to identify singlets and SSC-A vs. FSC-A used to gate on intact cells and gate boundaries were defined based on untreated cells and then AF-647+ cells quantified

Tick this box to confirm that a figure exemplifying the gating strategy is provided in the Supplementary Information.